A conceptual model for milling formations in biological aggregates

Ryan Lukeman, Yue-Xian Li, and Leah Edelstein-Keshet

Department of Mathematics, and Institute of Applied Mathematics

University of British Columbia, Vancouver, BC, Canada V6T 1Z2

September 4, 2008

Abstract

Collective behaviour of swarms and flocks has been studied from several perspectives, including continuous (Eulerian) and individual-based (Lagrangian) models. Here we use the latter approach to examine a minimal model for the formation and maintenance of group structure, with specific emphasis on a simple milling pattern in which particles follow one another around a closed circular path.

We explore how rules and interactions at the level of the individuals lead to this pattern at the level of the group. In contrast to many studies based on simulation results, our model is sufficiently simple that we can obtain analytical predictions. We consider a Newtonian framework with distance-dependent pairwise interaction force. Unlike some other studies, our mill formations do not depend on domain boundaries, nor on centrally attracting force-fields or rotor chemotaxis.

By focusing on a simple geometry and simple distant-dependent interactions, we characterize mill formations and derive existence conditions in terms of model parameters. An eigenvalue equation specifies stability regions based on properties of the interaction function. We explore this equation numerically, and validate the stability conclusions via simulation, showing distinct behaviour inside, outside, and on the boundary of stability regions. Moving mill formations are then investigated, showing the effect of individual autonomous self-propulsion on group-level motion. The simplified framework allows us to clearly relate individual properties (via model parameters) to group-level structure. These relationships provide insight into the more complicated milling formations observed in nature, and suggest design properties of artificial schools where such rotational motion is desired.

1 Introduction

In biological aggregates, there are many examples of group-level patterns that emerge from interactions among individuals. Such phenomena have motivated a number of modeling approaches aimed at connecting the interactions of individuals to the emergent collective behaviours. Lagrangian models, based on tracking the positions and velocities of individuals contrast with the Eulerian models, formulated in terms of reaction-transport equations. Examples of the Lagrangian approach include [Sakai(1973), Suzuki and Sakai(1973), Huth and Wissel(1992), Niwa(1994), Niwa(1996), Vicsek *et al.*(1995), Levine *et al.*(2001), Couzin *et al.*(2002), Mogilner *et al.*(2003), D'Orsogna *et al.*(2006)]. In the Lagrangian framework, each individual is described by several ordinary differential equations (for components of velocity and position in 1-3 spatial dimensions). This means that the complexity and size of the model increases proportionately to the size of the group, rendering such models notoriously difficult to understand analytically. Due to this inherent challenge, many previous Lagrangian models are largely dominated by simulation studies. Interesting patterns are found and classified, but an open question remains as to which aspects of a given model leads to which emergent feature of the group. Even when exhaustive search of parameter space is undertaken, linking classes of interaction functions to the types of patterns they form is a major challenge.

Motivated by the desire to obtain analytic results that characterize the link between individual interactions and the patterns formed by groups, we here explore a minimal model that has the advantage of analytic tractability. The goals of our paper are to further investigate a framework that is simple enough that we can unequivocally assess which properties of interaction functions, parameters, and rules lead to existence and stability of group patterns. Based on the challenges described above, such a task can only be done at this point on a restricted set of simple cases where we can exploit regularity of the pattern, symmetry properties, and limited coupling to achieve analytical power. Fortunately, simulations can be used to complement this analysis, and to expand insights to cases that cannot be solved in closed form.

Emergent patterns in nature can help to inform and validate models for group behaviour. One particular pattern that emerges in many of these models, and occasionally in nature, is the

milling formation (also known as a 'vortex formation'), in which individuals move in roughly concentric trajectories. In some previous models, milling mechanisms have been engineered in specific confined domains (due to interactions with boundaries), or by including "rotor chemotaxis" terms, representing a tendency to maintain some angle to the gradient of an attractive force-field. (We compare some previous examples in our Discussion.) Since many competing models can produce similar patterns, the emergence of a mill (or for that matter, any other pattern) can not be used to claim "correctness" of a given model. However, it is of interest to assess which attributes of a given model produce the resulting pattern. In this paper we explore what features of our minimal model would be consistent with existence and stability of mill formations.

In order to gain insight into the existence and stability properties of milling formations, we take the following approach: we consider a spatially simple solution that still captures the essential behaviour of milling, given by equally-spaced particles moving around a circle of fixed radius, at fixed angular velocity. These particles interact only via distance-dependent forces of attraction and repulsion, neglecting velocity-dependent forces common in similarly motivated models. We exploit the regularity of this idealized milling formation to address the following questions analytically: (i) Under what conditions on the school forces do such idealized formations occur (existence)? (ii) Given their existence, what further conditions guarantee that these patterns are not destroyed by random perturbations (stability)? Under this approach, we do not seek to realistically model the observed behaviours in nature (which are undoubtedly more complex), but instead seek to understand the connection between individual interaction and group stability via an abstraction of the milling phenomenon. Focusing on a simpler pattern while using a simple model leads to clear-cut results that can be derived analytically. This lends insight into the more complicated group structures found in nature.

Our approach is somewhat similar to [Marshall *et al.*(2004)] who consider similar formations from a multi-agent control system perspective, and derive stable steering controls for particles moving with fixed speed.

In a companion paper [Li *et al.*(2007)], a model for school formation was introduced based on the Lagrangian viewpoint, that is, following individual particles, rather than densities of organ-

isms. Equations of motion were formulated based on the Newtonian approach, i.e., describing changes in the velocities and positions of the particles under forces of propulsion and interaction. This self-propelled particle model was used to study *perfect schools*, which are configurations of particles in which the spacing is constant and identical, and where individuals in the group move at constant speed. One such perfect school in two dimensions, the *soldier formation*, was studied in [Li *et al.*(2007)] using linear stability analysis. Analytic stability bounds were found in terms of the slope of the interaction force as a function of interindividual distance. Numerical simulations were used to validate analytic conditions obtained, and investigate more complicated perfect schools. In this paper, we investigate milling formations using the same theoretical framework as described above.

Compared with linear aggregates [Li *et al.*(2007)], the dynamics of the milling formation are significantly more complicated. The dependence of stability on the slope of the interaction function evaluated at interindividual distance is given in terms of a complex-coefficient quartic polynomial. We investigate solutions to this equation numerically, classifying distinct behaviours in each stability regime. The structure of the interaction matrix that determines how individuals interact is crucial to the stability analysis; consequently, block circulant matrices and their properties enter heavily in our analysis.

In Section 2, we introduce the basic assumptions of the model and the differential equation system that describes the motion of the particles. We develop existence conditions for the mill formation in Section 3, and stability conditions in Section 4. In Section 5, existence and stability conditions are investigated numerically, through numerical solution to the eigenvalue equation, and through simulations. A discussion follows in Section 6.

Milling formations in nature

The milling formation is most often observed in schooling fish. This phenomenon was described by A. E. Parr in 1927 [Parr(1927)]. Numerous species of fish, including jack, barracuda, and tuna have been observed to mill in nature [Couzin *et al.*(2002)]. Photographs of jack milling in [Parrish and Edelstein-Keshet(1999), Parrish *et al.*(2002)] are presented as examples of emergent

Fig. 1: An example of milling in Atlantic bluefin tuna, courtesy of Dr. M. Lutcavage, Large Pelagics Research Center, UNH.

properties of fish schools. Milling tuna have been observed in the Gulf of Maine (see Figure 1), while barracuda mills abound in underwater photography. Basking sharks have also been observed in mills during courting behaviour [Harvey-Clark *et al.*(1999), Wilson(2004)].

Another example of milling is in army ants. In a thorough treatment, Schneirla [Schneirla(1944)] describes a rare field observation of *Eciton praedator* exhibiting milling behavior following a rain-induced separation of a group of ants from the main columnar raiding swarm. Although the sensory mechanism and environments differ from fishes to ants, in both cases individuals turn towards a dominant centripetal stimulation [Schneirla(1944)].

The above instances of milling in nature are self-organized in the sense that the global pattern emerges solely from interactions among individuals, using only local information [Camazine *et al.*(2001)]. Importantly, the occurrence of such mills is relatively rare in many instances, as they emerge (for example in ants) in unusual or extreme cases. (Schneirla [Schneirla(1944)] reports that ants in such mills follow one another to death by exhaustion.) Fortunately, given a wide variety of initial

conditions, army ants form trunk trail foraging patterns, rather than mills; but when a closed-loop topology occurs by chance, their mill is a stable and long-lasting movement pattern.

These observations raise an interesting question concerning the mechanisms that ensure the occurrence of self-organized milling patterns. The realistic mechanisms remain elusive since we know little about the actual rules of how animals interact. However, a number of models have been proposed in which milling patterns that closely resemble the observed mills have been shown to occur [Levine *et al.*(2001), D'Orsogna *et al.*(2006)]. Although experimental verifications are required to test whether these models are realistic, they provide insights into a number of mechanisms that are capable of producing milling.

2 The model of interacting self-propelled particles

The following basic assumptions apply to the idealized schools that we study in this paper.

(A1) All particles are identical and obey the same set of rules.

(A2) Particles are polarized, that is, each has a front and a back, and a particle senses other particles only in front of it. (This is a simplification of a classical assumption by [Huth and Wissel(1992)].)

(A3) The "effective force" experienced by one particle from a given neighbour depends only on distance.

(A4) A given particle interacts with its nearest neighbour(s). For analytic tractability we consider interactions with at most one neighbor.

(A5) The distance-dependent force between a pair of neighbours is a vector parallel to the line segment connecting the pair.

Consider a group of n self-propelled particles ($i = 1, 2, \ldots, n$), with position $\vec{x}_i$ and velocity $\vec{v}_i$. For simplicity, we assume that the body alignment of the i^{th} particle is identical to its direction of motion, i.e. the direction of $\vec{v}_i$. The movement of the i^{th} particle is governed by the classical

Newton's law of motion with equations

$$\dot{\vec{x}}_i = \vec{v}_i, \tag{1}$$

$$\dot{\vec{v}}_i = \vec{a}_i + \vec{f}_i - \gamma\vec{v}_i, \tag{2}$$

where $\dot{x} \equiv dx/dt$ denotes a derivative with respect to time and the mass of each individual is scaled so that $m_i = 1$ for all particles. $\vec{a}_i$ is an autonomous self-propulsion force generated by the i^{th} particle that may depend on environmental influences and on the location of the particle in the school. $\vec{f}_i$ is the interaction or schooling force that moves the i^{th} particle relative to its neighbour. The term $\gamma\vec{v}_i$ is a damping force with a constant drag coefficient ($\gamma > 0$) which assures that the velocity is bounded. Equation (2) implies that if a particle stops propelling, its velocity decays to zero at the rate γ. Particles are modeled in 2-dimensional space, so for a group of n particles, there are $4n$ first-order equations.

In the following analysis, $\vec{a}_i$ is a constant vector, identical for all particles. Based on the model assumptions (A3-A5), the schooling force is given by

$$\vec{f}_i = g(|\vec{x}_j - \vec{x}_i|)\frac{(\vec{x}_j - \vec{x}_i)}{|\vec{x}_j - \vec{x}_i|}, \tag{3}$$

where the index j refers to the nearest neighbour detected by particle i and $g(x)$ is a function of the absolute distance between particles (i.e., defined for $x > 0$) that gives the magnitude of the interaction force. To produce a nonzero spacing, $g(x)$ should typically be positive for large x and negative for small x, indicative of short-range repulsion and long-range attraction. This feature is universal in almost all models of aggregate formation. (See review of attraction-repulsion models in [Mogilner *et al.*(2003)].)

2.1 Relationship to previous models

The model presented by Equations (1)–(2) is well-known. It is discussed in [Okubo(1980), Okubo *et al.*(2001)] and attributed to schooling studied by [Sakai(1973)] and [Suzuki and Sakai(1973)].

We briefly compare to other models for self-propelled particles. For comparison, we write (1)–(2) as

$$\dot{\vec{x}}_i = \vec{v}_i, \tag{4}$$

$$\dot{\vec{v}}_i \;=\; \vec{f}_{aut} + \vec{f}_{int}, \tag{5}$$

where $\vec{f}_{aut}$ is the force that is generated autonomously by each individual and $\vec{f}_{int}$ that is generated due to the interaction with others. In [D'Orsogna *et al.*(2006), Chuang *et al.*(2007), Niwa(1994), Niwa(1996), Niwa(1998)], $\vec{f}_{aut} = (\alpha - \beta|\vec{v}_i|^2)\vec{v}_i$ was studied. This model was originally obtained by minimizing the specific energy cost of a swimming fish [Weihs(1974)]. In [Levine *et al.*(2001)], $\vec{f}_{aut} = \alpha\frac{\vec{v}_i}{|\vec{v}_i|} - \beta\vec{v}_i$ (in the case of no velocity averaging). In both cases, particles tend to a preferred characteristic speed in the absence of interaction (in the first case, $v = \sqrt{\alpha/\beta}$, while in the second, $v = \alpha/\beta$). In this paper, $f_{aut} = -\beta\vec{v}_i$, and so in the absence of interaction, the speed of particles decays to zero. For the force of interaction, in [D'Orsogna *et al.*(2006), Chuang *et al.*(2007), Levine *et al.*(2001)], f_{int} is chosen as an all-to-all coupled distance-dependent Morse-type interaction. In our analysis, we leave the form of f_{int} general, but choose a nearest-neighbour coupling over all-to-all coupling for analytical treatment. We note that the idealized mill formations considered here also occur when using the model equations of [D'Orsogna *et al.*(2006), Chuang *et al.*(2007), Levine *et al.*(2001)] under our nearest-neighbour interaction regime.

2.2 The milling formation

In a perfect mill, n particles move continuously around a circle of radius r_0 with constant angular velocity ω_0. The particles are equally spaced at distance d, labeled sequentially, with particle i sensing particle $i+1$, and particle n sensing particle 1. The sector angle defined by adjacent particles in the mill is $\theta = 2\pi/n$, where n is the number of particles (see Figure 2 for labeling conventions).

To simplify the presentation of our analysis, we set $\vec{a}_i = 0$ for all i; that is, particles experience no self-propelling force in the absence of interactions. Later, we discuss the case for nonzero $\vec{a}_i$. These assumptions lead to

$$\frac{d\vec{x}_i}{dt} = \vec{v}_i, \tag{6}$$

$$\frac{d\vec{v}_i}{dt} = \vec{f}_i(\vec{x}_{i+1} - \vec{x}_i) - \gamma\vec{v}_i, \tag{7}$$

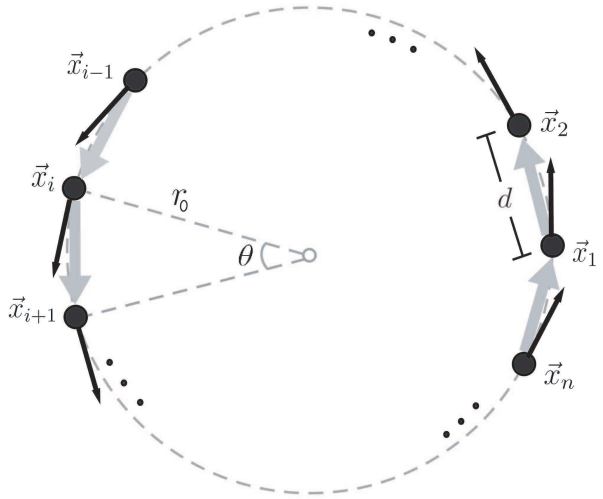

Fig. 2: A schematic diagram of the milling formation. Black arrows indicate direction of motion (tangential to the circle), while grey arrows indicate direction of schooling force.

for $i = 1, \ldots, n-1$, and

$$\frac{d\vec{x}_n}{dt} = \vec{v}_n, \tag{8}$$

$$\frac{d\vec{v}_n}{dt} = \vec{f}_n(\vec{x}_1 - \vec{x}_n) - \gamma\vec{v}_n. \tag{9}$$

Equations (8)–(9) link the n^{th} and 1^{st} particles into a (periodic) ring formation.

3 Existence conditions

The milling solution illustrated in Figure 2 represents a steady-state equidistant distribution of n particles on a ring of radius r_0 when observed in the frame that rotates at constant angular velocity ω_0. Solving (6)–(9) for such a steady state in the rotating frame yields r_0, ω_0, and interindividual distance d that uniquely determines such a milling solution. Here, we use a simple force-balance argument to obtain the same values. First, decompose the interaction force $\vec{f}$ into a component tangential to the circle, $\vec{f}_t$, and a centripetal component, denoted $\vec{f}_c$ (see Figure 3). In a steady-state mill solution, there is no linear acceleration, so tangential forces are in balance. Thus, for each particle,

$$\vec{f}_t - \gamma\vec{v} = 0. \tag{10}$$

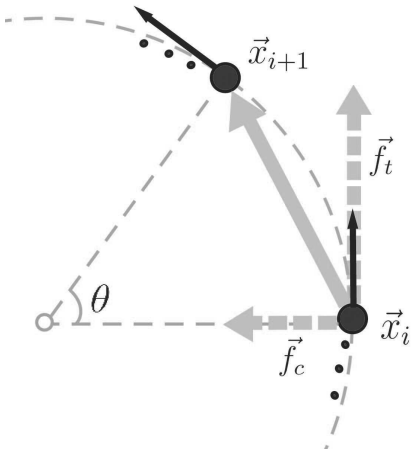

Fig. 3: A schematic diagram showing the decomposition of the interaction force into tangential and centripetal components.

The centripetal force that maintains the motion of a particle of mass $m = 1$ around a circle of radius r_0 at angular speed ω_0 is

$$\vec{f_c} = \vec{a}_c = \omega_0^2 r_0 \vec{u}_c,$$

where $\vec{u}_c$ is a radially-directed unit vector. Because $|\vec{v}| = r_0\omega_0$, we have

$$\vec{f_c} = \frac{|\vec{v}|^2}{r_0}\vec{u}_c. \tag{11}$$

Denote by ϕ and ψ the angles subtended to tangent and radius, respectively, as in Figure 4. Then $\theta = 2\pi/n$, $\phi = \theta/2 = \pi/n$, and $\psi = \pi/2 - \pi/n$. Using the law of cosines and simple trigonometry, we find that

$$d = 2r_0 \sin\left(\frac{\pi}{n}\right), \tag{12}$$

and express force magnitudes as

$$\begin{aligned} |f_t| &= g(d)\cos\left(\frac{\pi}{n}\right), \\ |f_c| &= g(d)\sin\left(\frac{\pi}{n}\right). \end{aligned}$$

Using (10) and (11),

$$g(d)\cos\left(\frac{\pi}{n}\right) = \gamma|\vec{v}|, \tag{13}$$

$$g(d)\sin\left(\frac{\pi}{n}\right) = \frac{|\vec{v}|^2}{r_0}, \tag{14}$$

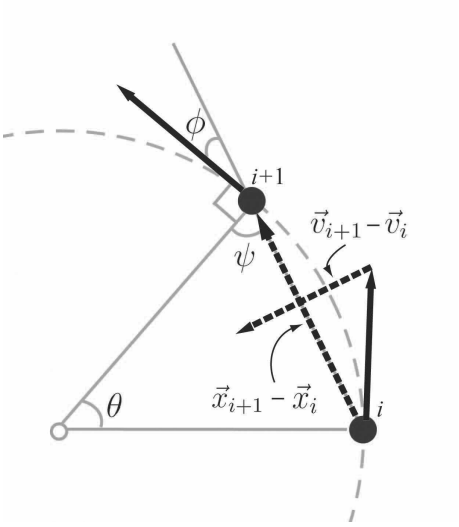

Fig. 4: A schematic diagram of particles in the mill formation showing angles introduced in the text, and relative position and velocity vectors.

and solving for $|\vec{v}|$ and r_0 gives

$$|\vec{v}| = \frac{g(d)\cos\left(\frac{\pi}{n}\right)}{\gamma}, \quad r_0 = \frac{g(d)\cos^2\left(\frac{\pi}{n}\right)}{\gamma^2 \sin\left(\frac{\pi}{n}\right)}. \tag{15}$$

Then angular frequency, ω_0 is related to speed and mill radius, r_0 by

$$\omega_0 = |\vec{v}|/r_0 = \gamma \tan\left(\frac{\pi}{n}\right). \tag{16}$$

For given $g(x)$, n and γ, (15) and (16) give the equilibrium radius and angular velocity of the milling formation. For an n-particle system, these quantities completely characterize the milling solution. Combining (12) and (15), we obtain the existence condition

$$g(d) = sd, \tag{17}$$

where $s = \gamma^2/2\cos^2\left(\frac{\pi}{n}\right)$. A steady-state mill formation occurs if and only if there exists a value of d satisfying (17) for a given function $g(x)$. Intersections of $g(d)$ and the straight line sd are mill formations. In Figure 5, intersections indicate potential steady-state values of d for which the mill formation can exist in [a], while in [b] absence of intersections indicate that a steady-state mill formation is not possible. Significantly, the slope s of the right-hand side of (17) affects

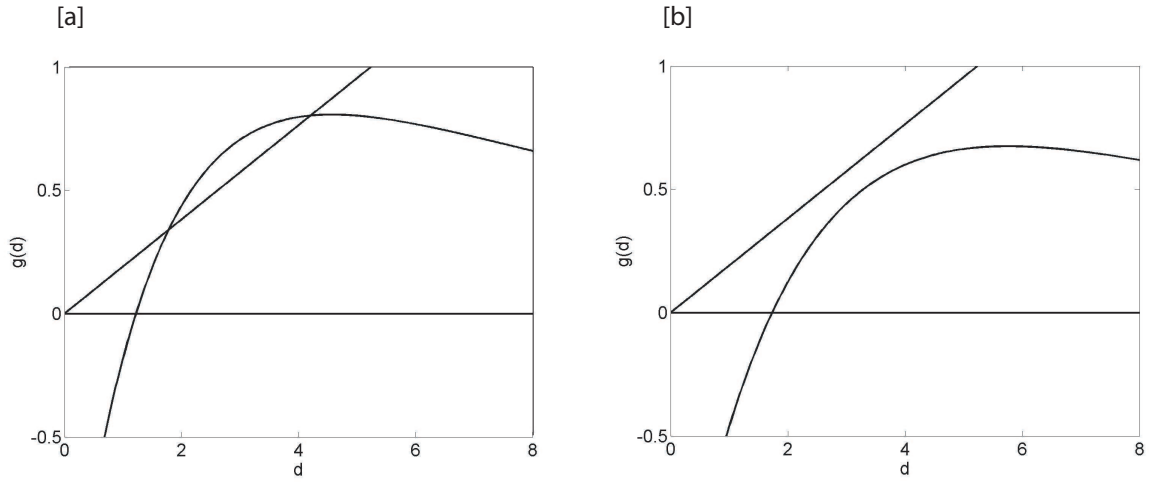

Fig. 5: Equation (17) represented graphically for $\gamma = 0.5$, $n = 5$, and $g(x) = A\exp(-x/a) - B\exp(-x/b)$. Horizontal axis: inter-individual distance d, vertical axis: distance-dependent force magnitude. $A = 1.5$, $a = 10$, $B = 3$. In panel [a], $b = 1.5$, and milling is possible whereas in panel [b], $b = 2$ and no milling solution exists.

whether or not an intersection exists. For typical $g(x)$, a shallower slope increases the likelihood of an intersection, so decreasing the damping coefficient γ or increasing the number of individuals n increases the likelihood of existence of the milling state. The dependence on n implies the possibility of a mill formation being destroyed when one or more particles leaves the group. Figure 6 shows a plot of Equation (17) for various values of n. In this example, for fewer than 5 particles, a mill solution will not exist.

4 Stability analysis

In this section, we investigate the local stability of the milling solution via a linear stability analysis. Our goal is to linearize (6)–(9) at the milling solution and study the eigenvalues that determine the stability of the solution. Here we exploit the simplifications and assumptions of the model, without which stability matrices become unwieldy. The cyclic nature of particle interactions is

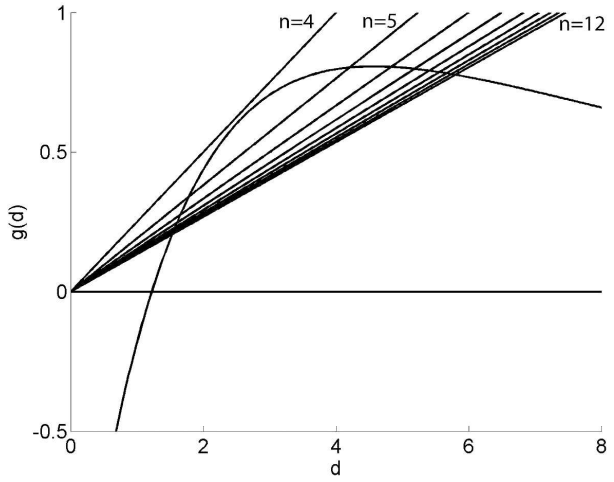

Fig. 6: A plot of the left-hand and right-hand sides of (17) for a range of n values, from $n = 4$ to $n = 12$. Note that no intersection occurs for $n = 4$, but two occur for $n = 5$.

reflected by a block-circulant structure in the stability matrix, which has the form

$$\begin{bmatrix} A_1 & A_2 & \cdots & A_n \\ A_n & A_1 & \cdots & A_{n-1} \\ & & \vdots & \\ A_2 & \cdots & A_n & A_1 \end{bmatrix},$$

where the A_i are $m \times m$ block matrices. Because an explicit formulation of the determinant is known for an $mn \times mn$ block-circulant matrix, we can exploit this structure in calculating eigenvalues. However, here we encounter a challenge: because $\vec{x}_{i+1} - \vec{x}_i$ terms appear in the stability matrix, and this vector has a different direction for each particle, successive rows of blocks are not identical modulo a shift. To overcome this issue, we transform coordinates. Let

$$\hat{\vec{x}}_i = R(\phi_i)\left(\vec{x}_{i+1} - \vec{x}_i\right), \tag{18}$$

$$\hat{\vec{v}}_i = R(\phi_i)\left(\vec{v}_{i+1} - \vec{v}_i\right), \tag{19}$$

where

$$R(\phi_i) = \begin{bmatrix} \cos(\phi_i) & \sin(\phi_i) \\ -\sin(\phi_i) & \cos(\phi_i) \end{bmatrix}, \tag{20}$$

is a rotation matrix with angle

$$\phi_i = \frac{2\pi i}{n} + \omega_0 t + \frac{\pi}{n} + \frac{\pi}{2}. \tag{21}$$

This transformation is best understood as a composition of a number of transformations. First, position and velocity differences are taken to simplify the system of equations. Second, these differences are rotated by the angle ϕ_i, transforming the system to a rotating frame. In this rotating frame, position and velocities appear to be fixed at the milling solution. Third, an index-dependent rotation of $2\pi i/n$ is applied to each particle so that steady-state quantities are independent of index (required for the circulant structure in the stability matrix). Last, a constant rotation of $\pi/n + \pi/2$ is applied so that the steady-state position and velocity vectors lie on the coordinate axes. We note that applying these three rotations does not affect eigenvalues because the linearized coefficient matrix and its analogue without rotation are similar matrices.

The transformed system of equations governing rotated position and velocity differences is

$$\frac{d}{dt}\hat{\vec{x}}_i = \omega_0 \mathbf{k} \times \hat{\vec{x}}_i + \hat{\vec{v}}_i, \tag{22}$$

$$\frac{d}{dt}\hat{\vec{v}}_i = \omega_0 \mathbf{k} \times \hat{\vec{v}}_i + R\left(\frac{-2\pi}{n}\right) \frac{\hat{\vec{x}}_{i+1}}{|\hat{\vec{x}}_{i+1}|} g\left(|\hat{\vec{x}}_{i+1}|\right) - \frac{\hat{\vec{x}}_i}{|\hat{\vec{x}}_i|} g\left(|\hat{\vec{x}}_i|\right) - \gamma \hat{\vec{v}}_i, \tag{23}$$

and steady-state values are given by

$$\hat{\vec{x}}_i^s = \hat{\vec{x}}^s = \begin{bmatrix} d \\ 0 \end{bmatrix}, \qquad \hat{\vec{v}}_i^s = \hat{\vec{v}}^s = \begin{bmatrix} 0 \\ \omega_0 d \end{bmatrix}, \tag{24}$$

for $i = 1, 2, \ldots, n$ with $n+1$ identified with 1 (see Appendix A for details). The extra rotation $R\left(\frac{-2\pi}{n}\right)$ in (23) is required to write this equation in terms of the transformed coordinates. Note that both $\hat{\vec{x}}_i^s$ and $\hat{\vec{v}}_i^s$ are independent of the index i; i.e., in this coordinate frame, all particles have the same steady-state coordinates $\hat{\vec{x}}^s$ and $\hat{\vec{v}}^s$. Next we introduce perturbations to the steady state milling solution in the transformed coordinate system; i.e.,

$$\hat{\vec{x}}_i = \hat{\vec{x}}^s + \vec{\delta}_i(t), \tag{25}$$

$$\hat{\vec{v}}_i = \hat{\vec{v}}^s + \vec{\xi}_i(t). \tag{26}$$

We substitute (25)–(26) into (22)–(23) and linearize interaction terms in (23). Then, taking together equations for all $i = 1, \ldots, n$, we can write the full perturbed linear system in matrix

notation. To facilitate this, we introduce a number of 2×2 matrices. We let

$$\mathbf{\Omega} = \begin{bmatrix} 0 & \omega_0 \\ -\omega_0 & 0 \end{bmatrix}, \ \mathbf{D} = \frac{\partial \vec{f}}{\partial \hat{\vec{x}}_i}|_{(d,0)} = \begin{bmatrix} g'(d) & 0 \\ 0 & g(d)/d \end{bmatrix}, \ \mathbf{RD} = R\left(\frac{-2\pi}{n}\right) \begin{bmatrix} g'(d) & 0 \\ 0 & g(d)/d \end{bmatrix}. \tag{27}$$

The full $4n \times 4n$ linear system is then

$$\frac{d}{dt}\begin{bmatrix} \vec{\delta}_1 \\ \vec{\delta}_2 \\ \vdots \\ \vec{\delta}_n \\ \vec{\xi}_1 \\ \vec{\xi}_2 \\ \vdots \\ \vec{\xi}_n \end{bmatrix} = \left[\begin{array}{cccc|cccc} \mathbf{\Omega} & & & & \mathbf{I} & & & \\ & \mathbf{\Omega} & & & & \mathbf{I} & & \\ & & \ddots & & & & \ddots & \\ & & & \mathbf{\Omega} & & & & \mathbf{I} \\ \hline -\mathbf{D} & \mathbf{RD} & & & \mathbf{\Omega} - \gamma\mathbf{I} & & & \\ & -\mathbf{D} & \mathbf{RD} & & & \ddots & & \\ & & \ddots & & & & \ddots & \\ \mathbf{RD} & & & -\mathbf{D} & & & & \mathbf{\Omega} - \gamma\mathbf{I} \end{array}\right] \begin{bmatrix} \vec{\delta}_1 \\ \vec{\delta}_2 \\ \vdots \\ \vec{\delta}_n \\ \vec{\xi}_1 \\ \vec{\xi}_2 \\ \vdots \\ \vec{\xi}_n \end{bmatrix}, \tag{28}$$

where $\mathbf{I}$ is the 2×2 identity matrix. The coefficient matrix is composed of four $n \times n$ block matrices, three of which are block-diagonal, and one of which is block-circulant. Each component is itself a 2×2 matrix. If we consider cases with interactions with two or more nearest neighbors, the structure of such matrices becomes intractable using our techniques. For the full derivation of (28), see Appendix B. We note that ω_0 is given explicitly in terms of n and γ in (16), and we can rearrange (17) to obtain

$$\frac{g(d)}{d} = s, \tag{29}$$

i.e., expressing $g(d)/d$ explicitly in terms of n and γ. Thus, we reduce the parameters in (28) to the drag coefficient γ, the number of particles n, and the slope of the interaction function at steady state, $g'(d)$.

4.1 Eigenvalues

We denote the coefficient matrix in (28) as $\mathbf{C}$, and solve the eigenvalues of $\mathbf{C}$ via

$$\det\left(\mathbf{C} - \lambda \mathbf{I}_{4n \times 4n}\right) = 0,$$

where $\mathbf{I}_{4n\times 4n}$ is the $4n\times 4n$ identity matrix. Now we use the following result from [Silvester(2000)]: given the block matrix

$$\left[\begin{array}{cc}\mathbf{A}_{1,1} & \mathbf{A}_{1,2}\\ \mathbf{A}_{2,1} & \mathbf{A}_{2,2}\end{array}\right],$$

where $\mathbf{A}_{1,1}, \mathbf{A}_{1,2}, \mathbf{A}_{2,1}$, and $\mathbf{A}_{2,2}$ are $m\times m$ matrices, if $\mathbf{A}_{1,1}$ and $\mathbf{A}_{1,2}$ commute, then

$$\det\left[\begin{array}{cc}\mathbf{A}_{1,1} & \mathbf{A}_{1,2}\\ \mathbf{A}_{2,1} & \mathbf{A}_{2,2}\end{array}\right] = \det\left[\mathbf{A}_{2,2}\mathbf{A}_{1,1} - \mathbf{A}_{2,1}\mathbf{A}_{1,2}\right]. \tag{30}$$

We partition $\mathbf{C} - \lambda\mathbf{I}_{4n\times 4n}$ into four $n\times n$ block matrices and apply the above theorem, noting that the corresponding upper left and upper right submatrices commute, to obtain the reduced determinant equation:

$$\det\left(\mathbf{C} - \lambda\mathbf{I}_{4n\times 4n}\right) = \det\left[\begin{array}{ccccccc}\Lambda+\mathbf{D} & -\mathbf{RD} & \mathbf{0} & \cdots & & \mathbf{0}\\ \mathbf{0} & \Lambda+\mathbf{D} & -\mathbf{RD} & \mathbf{0} & \cdots & \mathbf{0}\\ & & \ddots & & & \\ -\mathbf{RD} & \mathbf{0} & \cdots & & \mathbf{0} & \Lambda+\mathbf{D}\end{array}\right] = 0, \tag{31}$$

where $\mathbf{0}$ is the 2×2 zero matrix, and where we have defined

$$\begin{aligned}\Lambda \equiv (\mathbf{\Omega} - \lambda\mathbf{I})(\mathbf{\Omega} - (\gamma+\lambda)\mathbf{I}) &= \left[\begin{array}{cc}-\lambda & \omega_0\\ -\omega_0 & -\lambda\end{array}\right]\left[\begin{array}{cc}-\lambda-\gamma & \omega_0\\ -\omega_0 & -\lambda-\gamma\end{array}\right]\\ &= \left[\begin{array}{cc}\lambda(\lambda+\gamma)-\omega_0^2 & -\gamma\omega_0 - 2\lambda\omega_0\\ \gamma\omega_0 + 2\lambda\omega_0 & \lambda(\lambda+\gamma)-\omega_0^2\end{array}\right].\end{aligned} \tag{32}$$

Next, we use a diagonalization method for block-circulant matrices from [Davis(1979)]. The diagonalization matrix is given by Fourier matrices; for details see [Marshall *et al.*(2004)] or [Davis(1979)]. The resulting n 2×2 diagonal blocks are given by

$$\begin{aligned}D_1 &= \Lambda + \mathbf{D} + \mathbf{RD},\\ D_2 &= \Lambda + \mathbf{D} + \varpi\mathbf{RD},\\ D_3 &= \Lambda + \mathbf{D} + \varpi^2\mathbf{RD},\\ &\vdots\\ D_n &= \Lambda + \mathbf{D} + \varpi^{n-1}\mathbf{RD},\end{aligned}$$

where $\varpi = \exp(2\pi j/n)$, where $j = \sqrt{-1}$. Note that the powers of ϖ give the n roots of unity. Because the determinant of a block-diagonal matrix is the product of the determinants of the individual blocks, solutions to (31) are solutions to

$$\det D_1 \det D_2 \cdots \det D_n = 0,$$

i.e., the collection of solutions to

$$\det D_i = 0, \qquad i = 1, \ldots n. \tag{33}$$

Expanding the $(i+1)^{\text{th}}$ equation leads to a 4^{th}-order complex-coefficient polynomial

$$p(\lambda) = 0 \tag{34}$$

to be solved for eigenvalues λ (see Appendix C). Explicit solutions to this equation are not easily obtained. However, given parameter values for γ, n, and $g'(d)$, roots can be found numerically.

We have thus far avoided the $n = 3$ case. Because all three particles are equidistant in a mill formation, a particle can switch nearest neighbours under a small perturbation, breaking the connection topology. Thus the three-particle mill formation is inherently unstable to perturbations.

5 Numerical investigation

We are interested in restrictions on the interaction function that guarantee *stable* mill solutions, i.e., such that linear stability theory points to eigenvalues with negative real parts. Note that based on (33), the eigenvalue problem involves the matrices Λ, $\mathbf{R}$ and $\mathbf{DR}$. For fixed n and γ, these matrices depend only on $g(d)/d$ and $g'(d)$, and because at the milling steady state, $g(d)/d = s$, eigenvalues depend only on $g'(d)$. We thus numerically investigate stability with respect to $g'(d)$ by treating this quantity as a bifurcation parameter, with the remaining parameters, n and γ, fixed. In Figures 7 - 9, we plot the real part of λ, $\mathrm{Re}(\lambda)$, for each of the four solutions to Equation (34), for each of $i = 0, \ldots, n-1$, for a total of $4n$ eigenvalues. We note that for all values of n that were investigated, three eigenvalues with $\mathrm{Re}(\lambda) = 0$ existed: a zero eigenvalue, associated with the

rotational symmetry, and a pair of purely imaginary conjugates, associated with the translational invariance of the center of the mill within a rotating frame.

For Figure 7, $n = 4$. There is a range of values of $g'(d)$ in [-0.26,0.25] for which the real part of all eigenvalues are nonpositive, consistent with stability. In Figures (8) and (9), $n = 5$ and $n = 6$, respectively. In contrast to the previous case, the stable range of $g'(d)$ shrinks successively, from $[-0.11, 0.19]$ for $n = 5$, to $[-0.08, 0.17]$ for $n = 6$. These results suggest that the mill solution is unstable if the slope of the interaction function at d is either too large or too small (i.e., too steep). Stable mills exist when $g'(d) < 0$, evidently due to the circular geometry, as linear formations studied in [Li *et al.*(2007)] required that $g'(d) > 0$.

In each of these three cases, the upper limit of the stability region coincides with the value of $g(d)/d$ at steady state for each n, that is,

$$g'(d) < s, \tag{35}$$

for stable mills. (Specifically, for $\gamma = 0.5$, and $n = 4, 5, 6$, we get $g(d)/d = 0.25, 0.191$, and 0.166 respectively). In each of these cases, the stability boundary is determined by a branch of eigenvalues that crosses from negative to positive real parts at the boundary value of $g'(d)$. It can be shown analytically that a branch of $\mathrm{Re}(\lambda)$ crosses over the $g'(d)$ axis at $g(d)/d$ by examining coefficients of $p(\lambda)$ when $g'(d) = g(d)/d$. However, it remains to be proven that this crossover value always represents the upper-bound of the stability region. As n increases, we have found numerically that the lower bound on the stability region approaches 0.

5.1 Numerical simulations

A self-organized pattern in a dynamical system refers to a structurally stable solution that occurs as a result of interactions between individuals in a group [Levine *et al.*(2001), D'Orsogna *et al.*(2006), Li *et al.*(2007)] and does not occur as a result of forcing constraints asserted by other groups (e.g. predators) and/or the environment [Hemmingsson(1995), Grossman *et al.*(2008)]. Under the same interaction rules and model parameters, a number of stable self-organized patterns can occur and coexist. The emergence of one particular pattern is closely related to the initial state or

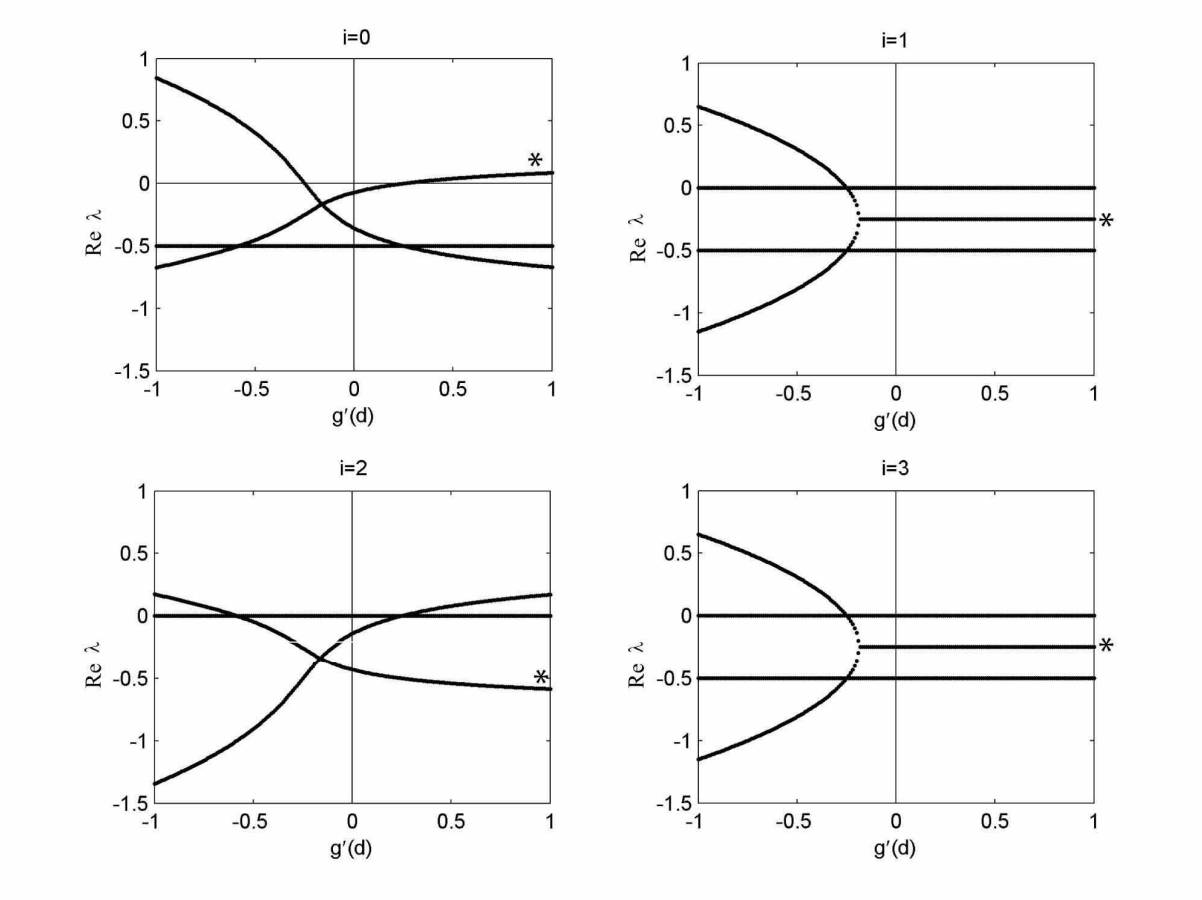

Fig. 7: Numerical solution to (34) over a range of values of $g'(d)$ for four particles ($n = 4$) and $\gamma = 0.5$. The real parts of eigenvalues are plotted for $i = 0, \ldots, 3$. The asterisks indicate branches of $\mathrm{Re}(\lambda)$ with multiplicity equal to 2. Note that the region over which all eigenvalues have non-positive real parts is approximately [-0.26,0.25].

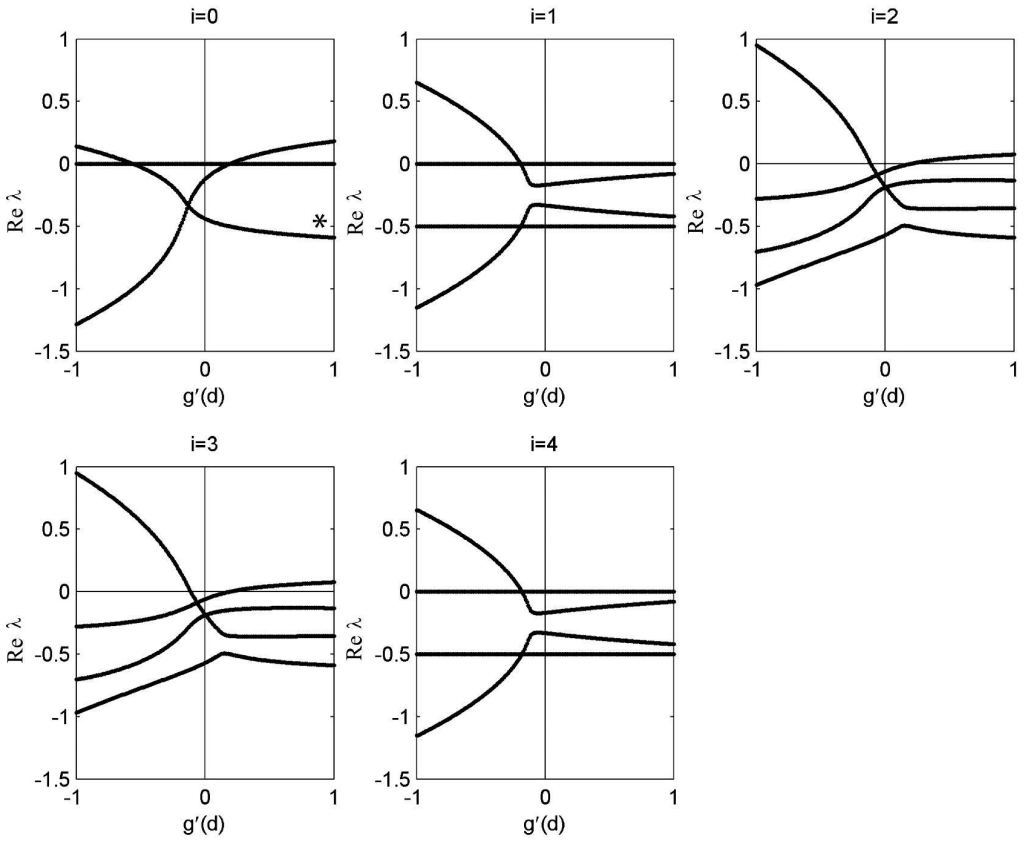

Fig. 8: As in Figure 7, but for five particles ($n = 5$). The real part of eigenvalues are plotted for $i = 0, \ldots, 4$. The region over which all eigenvalues have non-positive real parts is now approximately [-0.11,0.19].

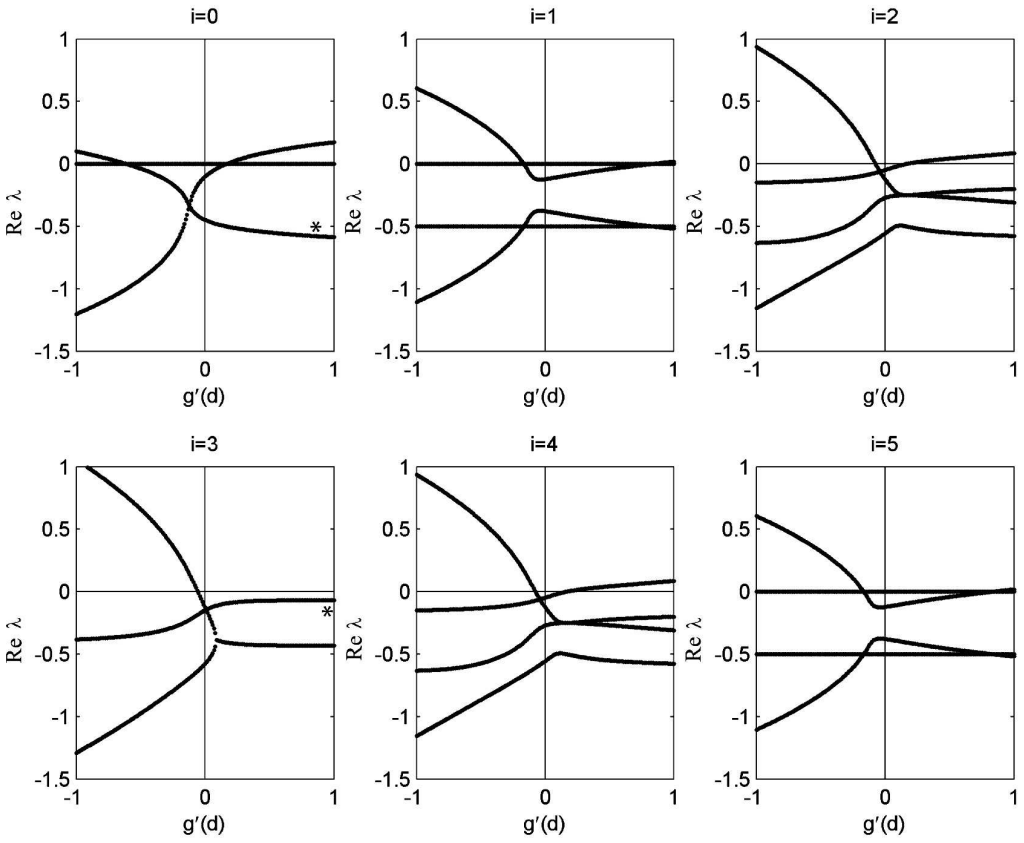

Fig. 9: As in Figure 7, but for six particles ($n = 6$). The real part of eigenvalues are plotted for $i = 0, \ldots, 5$. The region over which all eigenvalues have non-positive real parts is now approximately [-0.08,0.17].

configuration of the group. Large disturbances can also induce a switch from one pattern to another coexisting one. Mills that we studied in this model are obtained in simulations only when rather specific initial conditions were used, whereas most random initial conditions lead to other patterns. Therefore, they are self-organized patterns that occur under stringent initial configurations. This is consistent with the fact that milling is not the most commonly observed pattern in animal aggregates (as is the case in the example of milling army ants).

The particular restriction on initial conditions required for the emergence of a milling solution in (1)–(2) is that the nearest-neighbour connection topology of the group is a simple closed curve. To ensure this geometry, we chose initial positions to be equidistant individuals around a circle of fixed radius r, and then perturbed these (x, y) coordinates by values chosen randomly in $[-r/4, r/4]$. Initial velocities are tangential to the circle of radius r, with magnitude $\omega_0 r$. We point out that once this closed connection topology (with arbitrary geometry) is established in our simulations, the circular geometry that emerges is due only to local interactions among particles, without reference to any global information, and thus is self-organized [Camazine *et al.*(2001)].

The model equations (1)–(2) are evolved using ODE45 in MATLAB.

Figure 10 compares simulations of $n = 6$ particles in which Equation (17) has, versus does not have solutions. In Figure 10.a1, the left-hand and right-hand side of (17) are plotted, and intersections indicate individual distances d such that a mill formation can exist. However, our stability analysis indicates that the first intersection corresponds to an unstable solution because $g'(d) > s$. At the second intersection, the slope $g'(d)$ is within the range of stability, and as confirmed by Figure 10.a2, particles form a mill with spacing $d \approx 2$, and $r \approx 1.9$.

For the interaction function in Figure 10.b, no solution exists for (17). Corresponding simulations (Figure 10.b.ii) show particles initially forming a mill-like pattern; however, the radius of the group decreases until the individual distance d is such that $g(d) = 0$. At this stage, no further interactions occur, and the particles stop moving. We do not technically consider such stationary circular patterns to be "mills". In the case that there is no zero of the interaction function g, the group collapses to a point.

We now investigate the behaviour of the system at the boundary of stability, and inside the

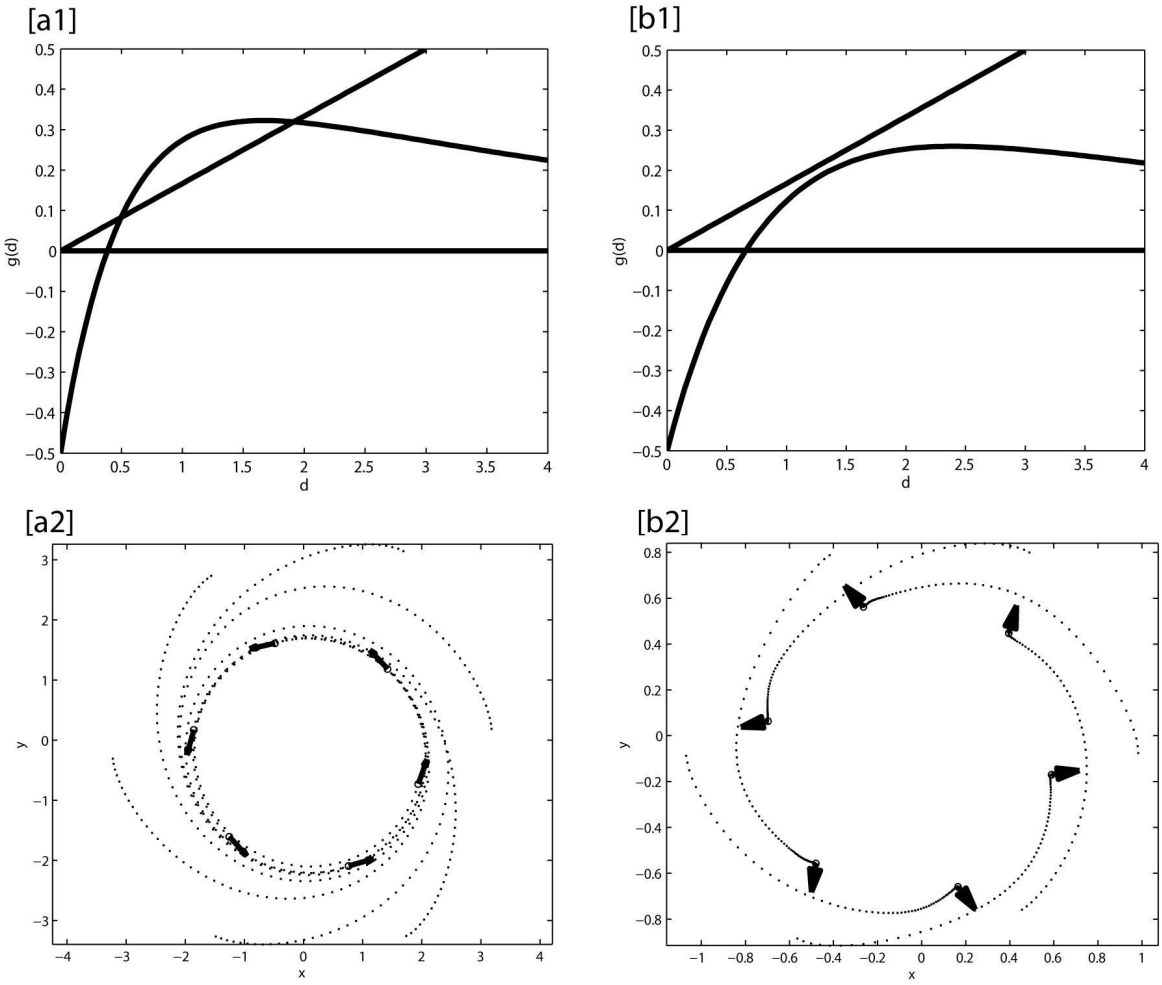

Fig. 10: A plot of the condition for mill solutions to exist [a1] or not [b1] given by Equation (17), and corresponding simulated particle tracks [a2] and [b2], with $\gamma = 0.5$. Note that in the case of an intersection, a stable mill forms at $d \approx 2$ (whereas $d \approx 0.5$ is unstable). However, when no intersection exists, the mill stops rotating and stationary particles are then arranged with d such that $g(d) = 0$ (final direction is outward due to small repulsive forces felt just before the particles stop). Arrows indicate direction facing at the end of the simulation. The interaction function used is as in Figure 5 with $A = 0.5$, $a = 5$, $B = 1$, and [a] $b = 0.5$, [b], $b = 0.8$.

region of instability. Earlier, we showed numerically that the system is stable over a region of $g'(d)$ which includes $g'(d) = 0$. Thus, choosing an interaction function whose slope at d is either too positive, or too negative, will result in instability in the mill solution. Just how this instability manifests itself can be seen in simulations. Figure 11.a1 shows an interaction function with two intersections indicating possible individual distances. However, at the first intersection, $g'(d)$ is too positive and Equation (35) is not satisfied (as indicated by the straight line), while at the second, $g'(d) \approx -0.10$ is too negative. Both values are outside the stability region [-0.07,0.17] noted in Figure 9 for $n = 6$. The corresponding simulation in Figure 11.a2 shows particles initially forming a circular group, though oscillations in individual distance grow until the connection topology is altered and the mill is broken. If $g(d)$ is linear with slope greater than s, we obtain a single intersection as in Figure 11.b1. In this case, simulations (Figure 11.b2) show a circular group forming, though the radius of the group grows exponentially in time, again confirming instability. Thus there are a number of ways in which the stability of the mill formation is lost, including radial increase in time, evolution to a stationary group, and breaking of the connection topology.

The system has yet a different behaviour with $g'(d)$ chosen to lie on the stability boundary. In this case, oscillations in individual distance d develop (as in the connection-breaking instability), but the oscillation magnitude approaches a fixed value and the system evolves to a new steady-state solution, the *irregular periodic mill*. Despite the periodic oscillation of distance between particles, the sum of the n distances between neighbouring particles is fixed when the irregular periodic mill is established. A plot of d in time showing this periodic behaviour is shown for one particle in an $n = 5$ system in Figure 12.a, while snapshots of the particles in time are shown in Figure 12.b.

5.2 Moving mill formations

In our treatment of mill formations up to this point, we have assumed that $\vec{a} = 0$; i.e., individuals are compelled to move only based on interactions with neighbours, and have no intrinsic desire to move in any direction. In this section, we explore the effect of assigning a non-zero autonomous self-propulsion to each individual.

In Figure 13, six particles initialized as usual, each with $\vec{a} = (0.1, 0.1)^T$, form a mill that moves

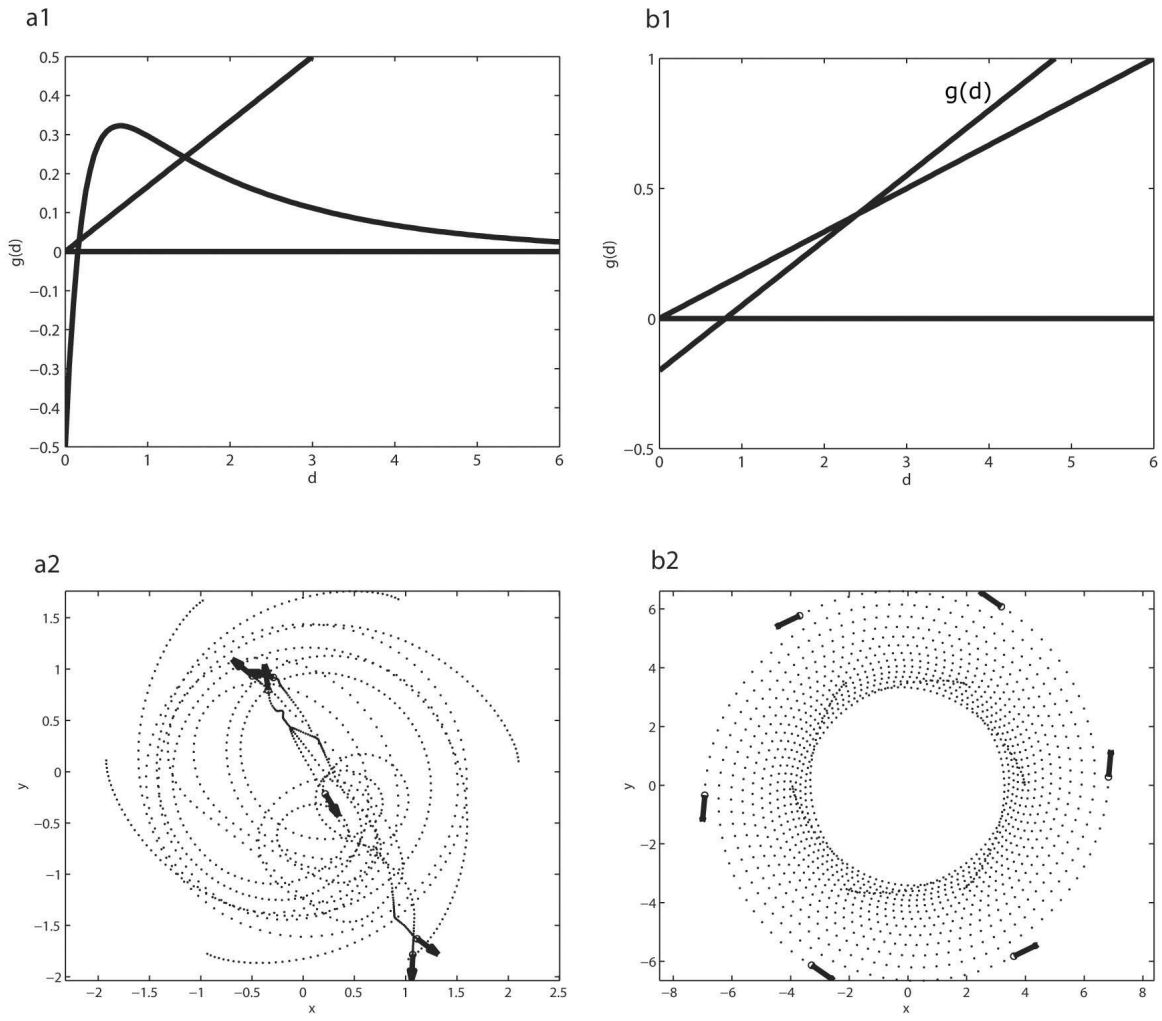

Fig. 11: [a1] An interaction function with $g'(d)$ lying outside the stability region for both intersections (implying no stable mill formation). Simulations using this function are shown in [a2]. Note that particles initially form a mill-like solution which is destroyed as time evolves. [b1] An interaction function with only one intersection, whose slope is too large ($g'(x) > s$ for all x). Simulations in [b2] show that the radius of the mill increases in time.

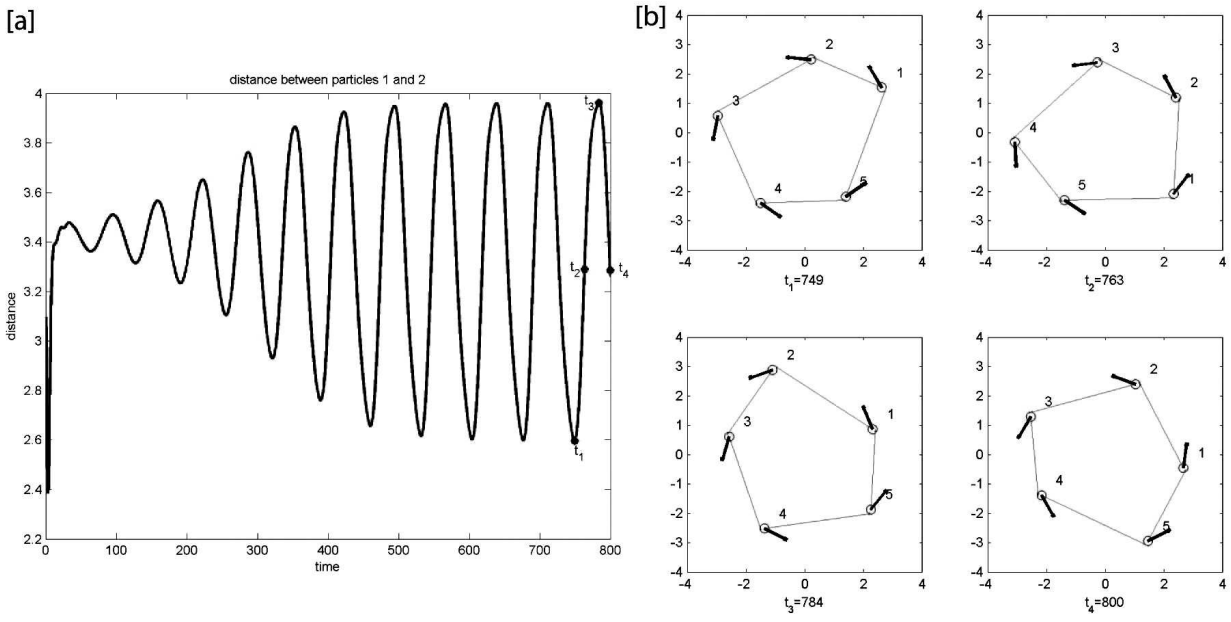

Fig. 12: The irregular periodic mill formation. [a] Individual distance d versus time for one particle in a system of 5 particles. For the 4 times denoted in [a], snapshots of particles are shown in [b], showing the variation in d between particles 1 and 2. The interaction function used was $g(x) = 1 - 0.11x$, so that $g'(d) = -0.11$ lies on the stability boundary.

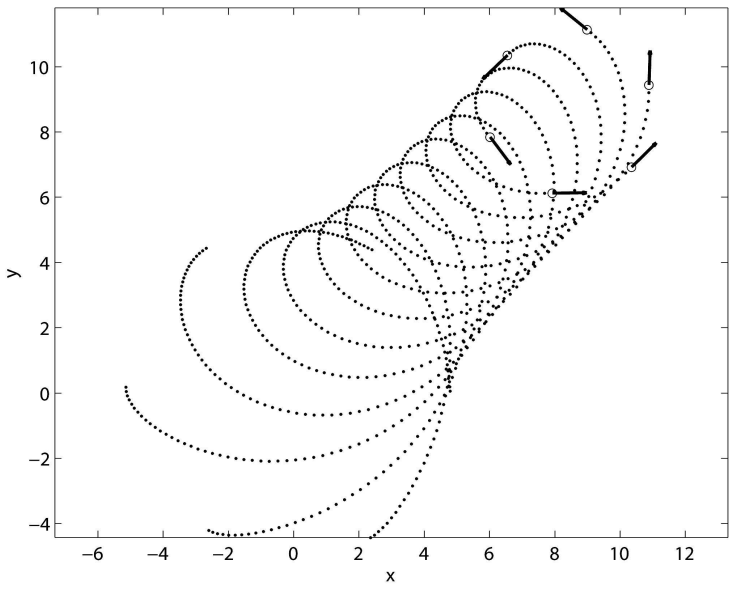

Fig. 13: A plot of trajectories in time for six particles with $\vec{a} = (0.1, 0.1)^T$. Note that the entire mill moves in the direction of $\vec{a}$.

in the direction of $\vec{a}$. Thus, autonomous self-propulsion in each individual acts to propel the entire mill along the direction of this individual propulsion. However, because the velocity of particles is now jointly composed of autonomous self-propulsion and interaction forces, the mill formation can be broken if $\vec{a}$ dominates the motion of individuals. Mill breaking occurs if some particle i no longer senses particle $i + 1$; i.e.,

$$\vec{v}_i^s \cdot \left(\vec{x}_{i+1}^s - \vec{x}_i^s \right) \leq 0. \tag{36}$$

Substituting known steady-state quantities in (36) and using some calculus, the mill-breaking condition reduces to

$$|\vec{a}| \geq g(d) \cos^2 \left(\frac{\pi}{n} \right), \tag{37}$$

(see Appendix D for derivation). In Figure 14.a, we set $\vec{a} = (0.223, 0.446)^T$, so that $|\vec{a}| = 0.498 < g(d) \cos^2 \left(\frac{\pi}{n} \right) = 0.5$, and a stable moving mill is formed. However, in Figure 14.b, a small increment in $\vec{a}$ to $(0.224, 0.448)^T$ gives $|\vec{a}| = 0.501 > 0.5$, resulting in a fundamental shift in behaviour: the mill formation breaks, and particles form a polarized group with a shift to $d \approx 2$ (see the inset of Figure 14.b). This new solution is consistent with those studied in [Li *et al.*(2007)]. In this example, the increase in the parameter $\vec{a}$ initiated a change in the connection topology of the

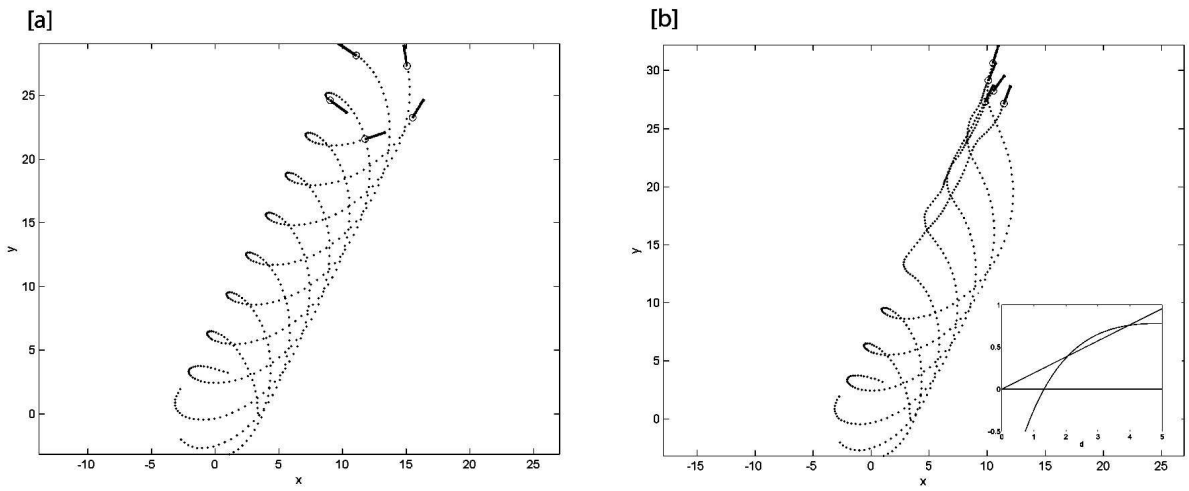

Fig. 14: A plot of trajectories in time for five particles with [a] $\vec{a} = (0.223, 0.446)^T$, and [b] $\vec{a} = (0.224, 0.448)^T$. Note that for a small parameter change, the system behaviour is fundamentally different. In these simulations, $g(x)$ is as in Figure 5, with $A = 1.5$, $a = 10$, $B = 3$, and $b = 1.6$. The corresponding existence condition is shown in the inset to [b].

particles, which in turn instigated an evolution to a different solution. Indeed, for any given set of parameters, there are a number of types of solutions that can occur; it is the arrangement of particles and headings that determines the solution to which the system converges.

6 Discussion

Milling formations exist in a number of biological aggregates, and provide fascinating examples of self-organized spatial patterns evolving from local interactions among individuals. Such patterns found occasionally in nature are irregular owing to heterogeneity in the population and environment, and likely more complex interactions. To reveal the cause-and-effect relationship between interaction properties and the patterns that emerge, we focused on idealized mill formations of particles rotating in a circular path of fixed radius. Although much simpler than the natural counterpart, this pattern permits mathematical analysis, which enabled us to make clear predictions of how model parameters influence the existence and stability of these patterns. Interactions in this model are distance-dependent, and so, likely, do not completely characterize the interactions in

natural mill formations. Yet, a detailed understanding of distance-dependent interactions should provide building blocks for understanding models incorporating more complex interactions.

Using a Lagrangian model based on Newton's equations of motion, we described mill formations in terms of group radius and angular velocity, and derived the following necessary condition for existence of a mill formation with spacing distance d, where γ is the drag coefficient, and n is the number of individuals:

$$g(d) = sd,$$

where $s = \gamma^2/2\cos^2(\pi/n)$. Increasing n, and/or decreasing γ increases the likelihood that the existence condition is satisfied.

A linear stability analysis on the milling formation resulted in block-circulant matrices that were block-diagonalized by Fourier matrices. This analysis could be done only in a limited, and particularly simple set of cases. Notably, the assumption of interactions with a single nearest neighbor was essential to limit the bandwidth of these matrices. The resulting determinant equation for eigenvalues yields a system of n complex-coefficient quartic polynomials, whose combined $4n$ solutions gives the spectrum of the stability matrix. Through numerical solution of these equations, stability bounds were found for particular cases of n and γ.

The geometry of the mill formation differs from soldier formations studied in [Li *et al.*(2007)] only through the n^{th} particle being connected to the first particle. Yet, remarkably, this connection adds considerable complexity to the issue of stability of the system. The most interesting stability dependence was seen in the slope of the interaction function at steady-state, $g'(d)$. A series of ranges were computed numerically for fixed γ and various values of n. We found numerically that as n increases, the region of stability decreases, asymptotic to $[0, \gamma^2/2]$. Interestingly, we found that increasing γ (or decreasing n) increases the stability region, but decreases the likelihood of a mill formation existing.

Unlike linear schools studied in [Li *et al.*(2007)], stable solutions can exist when $g'(d) < 0$. This is nonintuitive, as $g'(d) < 0$ means that a given particle i has a weaker attraction as it moves away from its neighbour to the front, $i+1$. This would seemingly inhibit restoring the steady-state milling solution. However, the circulant connection of particles must compensate for this weaker

attraction by inducing the particle to the back, $i-1$, to be more strongly attracted to particle i, and as this stronger "pull" propagates successively back around the mill, the attraction of particle i to $i+1$ is increased, imparting a stabilizing effect.

Numerical simulations validated our calculation of stability regions. Numerous routes to instability can occur, including evolution to a motionless steady-state, unbounded increase in radius, and breaking the circulant connection topology. Simulations of the system at the boundary of stable and unstable regions of $g'(d)$ indicated the existence a new type of solution, the irregular periodic mill, featuring a stable limit cycle in interindividual distances, resulting in a rotating, irregular, dynamic polygon of individuals with side lengths oscillating in time. Inclusion of an autonomous self-propulsion term, $\vec{a}$, for each particle was shown to move the entire mill in the direction of $\vec{a}$, until $|\vec{a}| \geq g(d)\cos^2\left(\frac{\pi}{n}\right)$, beyond which milling formations evolved to polarized groups similar to those studied in [Li *et al.*(2007)].

The model used in this paper is similar to other established self-propelled particle models as noted earlier. Slightly different interaction forces were used by some studies [D'Orsogna *et al.*(2006), Chuang *et al.*(2007), Niwa(1994), Niwa(1996), Niwa(1998), Levine *et al.*(2001)]. In some of these particles tend to a preferred characteristic speed in the absence of interaction. As our results are analytical and not just numeric, we could consider a more general interaction function f_{int} than adopted in other papers. However, this comes at the expense of restricting attention to (single) nearest-neighbour coupling over all-to-all coupling. Furthermore, our particles sense others only in the forward direction, an assumption which can be thought of as a generalization of the 'blind zone' assumptions of fish models (e.g., [Huth and Wissel(1992), Couzin *et al.*(2002)]). Our choice of a 180° blind zone could be reduced while still maintaining our mill stability results, so long as the blind zone width is sufficient to prevent a perturbed individual at the back being sensed, breaking the connection topology essential for maintaining the mill. Both the all-to-all coupling and our choice of coupling is likely unrealistic for most naturally occurring mills, yet both frameworks lend insight into the phenomenon.

As outlined in the introduction, many other competing models can give rise to mills. Milling formations emerge in these models through a number of mechanisms, and an interesting com-

parison can be made between our mills and those produced by others types of models. In [Czirók *et al.*(1996), Ben-Jacob *et al.*(1997)], an individual-based model for collective motion of bacteria is used to generate 'vortices' via a *rotor chemotaxis* term in the equations of motion. Including such terms in individual-based ODE's explicitly enforces rotation: particles moving tangentially to a unimodal attractant source distribution or central force field would exhibit rotational motion. Milling can be generated via an external environmental gradient, as is the case in the individual-based model of swarming *Daphnia* in [Mach and Schweitzer(2007)]. Milling can also emerge in models where particles have a non-zero equilibrium speed in a closed domain; such is the case in the coupled lattice map model of [Hemmingsson(1995)] and the spring-dashpot model used in [Grossman *et al.*(2008)]. Meanwhile, several models have exhibited milling solutions using only interactions among individuals; this can occur in all-to-all coupled distance- and velocity-dependent interactions [Levine *et al.*(2001)], or distance-dependent interactions only [Chuang *et al.*(2007), Levine *et al.*(2001)]. In [Couzin *et al.*(2002)], interactions between individuals are restricted to localized 'zones' of attraction, repulsion and alignment, and yet mill formations emerge in certain parameter regimes. From a continuum perspective, in [Topaz and Bertozzi(2004), Kulinskii *et al.*(2005), Csahók and Czirók(2008)] population density models have vortex-type formations as solutions.

The milling formations that emerge in the individual-based models discussed above are often qualitatively similar to such formations observed in nature. In [D'Orsogna *et al.*(2006)], conditions are derived that determine the *H-stability* of milling solutions (that is, whether or not the group will collapse to a point as more and more individuals are added). Also, milling formations have been stable to small amounts of noise in numerous studies. However, the analytical determination of conditions under which such formations exist and are stable to perturbations of its members remains unanswered due to the spatial complexity of these formations. Passing to the continuum limit often facilitates analysis by a reduction in order of the system, but this occurs at the cost of individual properties in favor of mean field properties. In [Ratushnaya *et al.*(2007)], a linear stability analysis was performed on a vortex-type solution of a continuum model, but was inconclusive.

It is not clear if any functional benefit is associated with milling formations in nature, or if

these are epiphenomena that result from aggregation in special circumstances. In any case, our results on the relationship between model parameters and observed formations may prove useful in furthering the qualitative understanding of these formations. Furthermore, our results are useful for the design of artificial schools (i.e., multi-agent systems) where such rotational coordinated motion is desired, as our modeling framework and stability results provide a simple and robust method of programming such agents.

Future work will include obtaining analytical stability bounds on $g'(d)$, which have been presented numerically here. An interesting extension of this work would be to investigate the effect of a velocity-dependent interaction in addition to the distance-dependent interactions studied here. Such an extension would result in a more realistic model for natural groups. As one considers more complicated formations of particles, the issue of labeling particles and determining their interaction topology may present a considerable challenge.

Acknowledgements This work was funded by NSERC discovery grants to Y.X. Li and L. Edelstein-Keshet. R. Lukeman was funded by an NSERC CGS-D scholarship and by the latter source. The authors are grateful to Chen Greif and Maria-Rita D'Orsogna for helpful discussions.

Appendices

A Transformation to relative coordinates

Expanding (18)–(19) gives

$$\hat{x}_i = \cos\phi_i\,(x_{i+1} - x_i) + \sin\phi_i\,(y_{i+1} - y_i)\,, \tag{38}$$

$$\hat{y}_i = -\sin\phi_i\,(x_{i+1} - x_i) + \cos\phi_i\,(y_{i+1} - y_i)\,, \tag{39}$$

$$\hat{u}_i = \cos\phi_i\,(u_{i+1} - u_i) + \sin\phi_i\,(v_{i+1} - v_i)\,, \tag{40}$$

$$\hat{v}_i = -\sin\phi_i\,(u_{i+1} - u_i) + \cos\phi_i\,(v_{i+1} - v_i)\,, \tag{41}$$

where $\vec{x}_i = (x_i, y_i)$, and $\vec{v}_i = (u_i, v_i)$. We can obtain the first model equation through time-differentiation of $\hat{x}_i$ and $\hat{y}_i$, which gives

$$\begin{aligned}
\frac{d}{dt}\hat{x}_i &= -\omega_0 \sin\phi_i\,(x_{i+1} - x_i) + \cos\phi_i\,(\dot{x}_{i+1} - \dot{x}_i) + \omega_0 \cos\phi_i\,(y_{i+1} - y_i) + \sin\phi_i\,(\dot{y}_{i+1} - \dot{y}_i)\,, \\
\frac{d}{dt}\hat{y}_i &= -\omega_0 \cos\phi_i\,(x_{i+1} - x_i) - \sin\phi_i\,(\dot{x}_{i+1} - \dot{x}_i) - \omega_0 \sin\phi_i\,(y_{i+1} - y_i) + \cos\phi_i\,(\dot{y}_{i+1} - \dot{y}_i)\,.
\end{aligned}$$

Using (38)–(41), we rewrite the above in the more compact vector notation

$$\frac{d}{dt}\hat{\vec{x}}_i = \hat{\vec{v}}_i + \omega_0 \mathbf{k} \times \hat{\vec{x}}_i, \tag{42}$$

where

$$\mathbf{k} \times \hat{\vec{x}}_i = \det \begin{bmatrix} \mathbf{i} & \mathbf{j} & \mathbf{k} \\ \hat{x}_i & \hat{y}_i & 0 \\ 0 & 0 & 1 \end{bmatrix} = (\hat{y}_i, -\hat{x}_i).$$

Similarly, we time-differentiate (40)–(41), giving

$$\dot{\hat{u}}_i = -\omega_0 \sin\phi_i\,(u_{i+1} - u_i) + \cos\phi_i\,(\dot{u}_{i+1} - \dot{u}_i) + \omega_0 \cos\phi_i\,(v_{i+1} - v_i) + \sin\phi_i\,(\dot{v}_{i+1} - \dot{v}_i)\,, \tag{43}$$

$$\dot{\hat{v}}_i = -\omega_0 \cos\phi_i\,(u_{i+1} - u_i) - \sin\phi_i\,(\dot{u}_{i+1} - \dot{u}_i) - \omega_0 \sin\phi_i\,(v_{i+1} - v_i) + \cos\phi_i\,(\dot{v}_{i+1} - \dot{v}_i)\,. \tag{44}$$

This can be rewritten more compactly using (40)–(41) as

$$\begin{aligned}\dot{\hat{\vec{v}}}_i &= \omega_0 \mathbf{k} \times \hat{\vec{v}}_i + R(\phi_i)\left(\dot{\vec{v}}_{i+1} - \dot{\vec{v}}_i\right) \\ &= \omega_0 \mathbf{k} \times \hat{\vec{v}}_i + R(\phi_i)\left(\vec{f}\left(\vec{x}_{i+2} - \vec{x}_{i+1}\right) - \vec{f}\left(\vec{x}_{i+1} - \vec{x}_i\right)\right) - R(\phi_i)\gamma\left(\vec{v}_{i+1} - \vec{v}_i\right). \end{aligned} \tag{45}$$

Following (3), we write the interaction force terms in (45) in terms of unit direction vectors and magnitudes:

$$\begin{aligned}R(\phi_i)\left(\vec{f}\left(\vec{x}_{i+2} - \vec{x}_{i+1}\right) - \vec{f}\left(\vec{x}_{i+1} - \vec{x}_i\right)\right) &= R(\phi_i)\frac{\left(\vec{x}_{i+2} - \vec{x}_{i+1}\right)}{\left|\vec{x}_{i+2} - \vec{x}_{i+1}\right|} g\left(\left|\vec{x}_{i+2} - \vec{x}_{i+1}\right|\right) \\ &\quad - R(\phi_i)\frac{\left(\vec{x}_{i+1} - \vec{x}_i\right)}{\left|\vec{x}_{i+1} - \vec{x}_i\right|} g\left(\left|\vec{x}_{i+1} - \vec{x}_i\right|\right). \end{aligned} \tag{46}$$

We make a number of observations. First, the rotational matrix operator R is distance-preserving, and so

$$\left|\vec{x}_{i+1} - \vec{x}_i\right| = \left|\hat{\vec{x}}_i\right|.$$

Second,

$$R(a)R(b) = R(a+b).$$

We use this property to recast (46), using (18), as

$$\begin{aligned}&R(\phi_i)\frac{\left(\vec{x}_{i+2} - \vec{x}_{i+1}\right)}{\left|\vec{x}_{i+2} - \vec{x}_{i+1}\right|} g\left(\left|\vec{x}_{i+2} - \vec{x}_{i+1}\right|\right) - R(\phi_i)\frac{\left(\vec{x}_{i+1} - \vec{x}_i\right)}{\left|\vec{x}_{i+1} - \vec{x}_i\right|} g\left(\left|\vec{x}_{i+1} - \vec{x}_i\right|\right) \\ &\qquad = R\left(\frac{-2\pi}{n}\right)\frac{\hat{\vec{x}}_{i+1}}{\left|\hat{\vec{x}}_{i+1}\right|} g\left(\left|\hat{\vec{x}}_{i+1}\right|\right) - \frac{\hat{\vec{x}}_i}{\left|\hat{\vec{x}}_i\right|} g\left(\left|\hat{\vec{x}}_i\right|\right), \end{aligned}$$

where we have used $R^{-1}(a) = R(-a)$. We now write the equation system in relative coordinates:

$$\dot{\hat{\vec{x}}}_i = \omega_0 \mathbf{k} \times \hat{\vec{x}}_i + \hat{\vec{v}}_i, \tag{47}$$

$$\dot{\hat{\vec{v}}}_i = \omega_0 \mathbf{k} \times \hat{\vec{v}}_i + R\left(\frac{-2\pi}{n}\right)\frac{\hat{\vec{x}}_{i+1}}{\left|\hat{\vec{x}}_{i+1}\right|} g\left(\left|\hat{\vec{x}}_{i+1}\right|\right) - \frac{\hat{\vec{x}}_i}{\left|\hat{\vec{x}}_i\right|} g\left(\left|\hat{\vec{x}}_i\right|\right) - \gamma\hat{\vec{v}}_i. \tag{48}$$

Next, we calculate the steady-state quantities. In equations (38)–(39), we replace the steady-state expressions for x_i, x_{i+1}, y_i and y_{i+1} to obtain

$$\hat{x}_i^s = -\cos\phi_i\left(r_0\cos\left(\hat{\theta}_i + \frac{2\pi}{n}\right) - r_0\cos\hat{\theta}_i\right) - \sin\phi_i\left(r_0\sin\left(\hat{\theta}_i + \frac{2\pi}{n}\right) - r_0\sin\hat{\theta}_i\right), \tag{49}$$

$$\hat{y}_i^s = \sin\phi_i\left(r_0\cos\left(\hat{\theta}_i + \frac{2\pi}{n}\right) - r_0\cos\hat{\theta}_i\right) - \cos\phi_i\left(r_0\sin\left(\hat{\theta}_i + \frac{2\pi}{n}\right) - r_0\sin\hat{\theta}_i\right), \tag{50}$$

where $\hat{\theta}_i = 2\pi i/n + \omega_0 t$. These expressions can be simplified using trigonometric difference formulas to

$$\hat{x}_i^s = -r_0 \cos\left(\phi_i - \hat{\theta}_i - \frac{2\pi}{n}\right) + r_0 \cos\left(\phi_i - \hat{\theta}_i\right),$$
$$\hat{y}_i^s = r_0 \sin\left(\phi_i - \hat{\theta}_i - \frac{2\pi}{n}\right) + r_0 \sin\left(\hat{\theta}_i - \phi_i\right),$$

which we can further simplify using the definition of ϕ_i in (21) to

$$\hat{x}_i^s = -r_0 \cos\left(-\frac{\pi}{2} - \frac{\pi}{n}\right) + r_0 \cos\left(\frac{\pi}{n} - \frac{\pi}{2}\right),$$
$$\hat{y}_i^s = r_0 \sin\left(-\frac{\pi}{2} - \frac{\pi}{n}\right) + r_0 \sin\left(-\frac{\pi}{n} + \frac{\pi}{2}\right).$$

With some simple trigonometric manipulation, we write

$$\hat{x}_i^s = -r_0 \sin\left(-\frac{\pi}{n}\right) + r_0 \sin\left(\frac{\pi}{n}\right),$$
$$\hat{y}_i^s = -r_0 \cos\left(-\frac{\pi}{n}\right) + r_0 \cos\left(\frac{\pi}{n}\right),$$

i.e.,

$$\hat{x}_i^s = 2r_0 \sin\left(\frac{\pi}{n}\right) = d, \tag{51}$$
$$\hat{y}_i^s = 0. \tag{52}$$

The steady-state positions in this coordinate frame are independent of the index i, and each position is a vector parallel to the x-axis with magnitude d, the interindividual distance at steady state in the original coordinates. Instead of calculating $\hat{u}_i^s$ and $\hat{v}_i^s$ directly as we did with position, we can evaluate (47) at steady state, which implies that

$$\hat{\vec{v}}_i^s = -\omega_0 \mathbf{k} \times \hat{\vec{x}}_i^s,$$

i.e.,

$$\hat{u}_i^s = 0,$$
$$\hat{v}_i^s = \omega_0 d,$$

both of which are independent of index.

B Derivation of the linearized perturbed system

Substituting (25)–(26) into (22)–(23) gives

$$\begin{aligned}
\frac{d}{dt}\left(\hat{\vec{x}}_i^s + \vec{\delta}_i(t)\right) &= \omega_0\mathbf{k}\times\left(\hat{\vec{x}}_i^s + \vec{\delta}_i(t)\right) + \hat{\vec{v}}_i^s + \vec{\xi}_i(t), &(53)\\
\frac{d}{dt}\left(\hat{\vec{v}}_i^s + \vec{\xi}_i(t)\right) &= \omega_0\mathbf{k}\times\left(\hat{\vec{v}}_i^s + \vec{\xi}_i(t)\right) - R_-\left(\frac{-2\pi}{n}\right)\vec{f}\left(\hat{\vec{x}}_{i+1}^s + \vec{\delta}_{i+1}(t)\right) &(54)\\
&\quad -\vec{f}\left(\hat{\vec{x}}_i^s + \vec{\delta}_i(t)\right) - \gamma\left(\hat{\vec{v}}_i^s + \vec{\xi}_i(t)\right),
\end{aligned}$$

where $i = 1,\ldots,n$, and $n+1$ is identified with 1 (henceforth assumed to be the case). Because $\mathbf{k}\times(\vec{a}+\vec{b}) = \mathbf{k}\times\vec{a} + \mathbf{k}\times\vec{b}$, (53) can be separated into steady-state and perturbed components. Using

$$\omega_0\mathbf{k}\times\hat{\vec{x}}_i^s + \hat{\vec{v}}_i^s = 0,$$

(53) can be simplified to

$$\frac{d}{dt}\vec{\delta}_i = \omega_0\mathbf{k}\times\vec{\delta}_i + \hat{\vec{\xi}}_i, \tag{55}$$

where we have dropped arguments of $\vec{\delta}_i$ and $\vec{\xi}_i$. We expand the nonlinear interaction terms in (54) via a linear approximation:

$$\begin{aligned}
R\left(\frac{-2\pi}{n}\right)\vec{f}\left(\hat{\vec{x}}_{i+1}^s + \vec{\delta}_{i+1}(t)\right) - \vec{f}\left(\hat{\vec{x}}_i^s + \vec{\delta}_i(t)\right) &\approx R\left(\frac{-2\pi}{n}\right)\left(f\left(\hat{\vec{x}}_{i+1}^s\right) + \frac{\partial\vec{f}}{\partial\hat{\vec{x}}_i}|_{(d,0)}\vec{\delta}_{i+1}\right)\\
&\quad -\vec{f}\left(\hat{\vec{x}}_i^s\right) - \frac{\partial\vec{f}}{\partial\hat{\vec{x}}_i}|_{(d,0)}\vec{\delta}_i.
\end{aligned}$$

Using this expansion in (54) and noting that

$$\omega_0\mathbf{k}\times\left(\hat{\vec{v}}_i^s\right) + R\left(\frac{-2\pi}{n}\right)\vec{f}\left(\hat{\vec{x}}_{i+1}^s\right) - \vec{f}\left(\hat{\vec{x}}_i^s\right) - \gamma\left(\hat{\vec{v}}_i^s\right) = 0,$$

we simplify (54) as

$$\frac{d}{dt}\vec{\xi}_i = \omega_0\mathbf{k}\times\vec{\xi}_i + R\left(\frac{-2\pi}{n}\right)\left(\frac{\partial\vec{f}}{\partial\hat{\vec{x}}_i}|_{(d,0)}\vec{\delta}_{i+1}\right) - \frac{\partial\vec{f}}{\partial\hat{\vec{x}}_i}|_{(d,0)}\vec{\delta}_i - \gamma\vec{\xi}_i.$$

Combining with (55), we now write the set of equations for the perturbed system:

$$\begin{aligned}
\frac{d}{dt}\vec{\delta}_i &= \omega_0\mathbf{k}\times\vec{\delta}_i + \hat{\vec{\xi}}_i, &(56)\\
\frac{d}{dt}\vec{\xi}_i &= \omega_0\mathbf{k}\times\vec{\xi}_i + R\left(\frac{-2\pi}{n}\right)\left(\frac{\partial\vec{f}}{\partial\hat{\vec{x}}_i}|_{(d,0)}\vec{\delta}_{i+1}\right) - \frac{\partial\vec{f}}{\partial\hat{\vec{x}}_i}|_{(d,0)}\vec{\delta}_i - \gamma\vec{\xi}_i. &(57)
\end{aligned}$$

We explicitly calculate the Jacobian matrix $\frac{\partial \vec{f}}{\partial \hat{\vec{x}}_i}$ by expanding $\vec{f}$ as in (48), i.e.,

$$\vec{f}(\hat{\vec{x}}_i) = \frac{\hat{x}_i}{|\hat{\vec{x}}_i|} g\left(|\hat{\vec{x}}_i|\right) \mathbf{i} + \frac{\hat{y}_i}{|\hat{\vec{x}}_i|} g\left(|\hat{\vec{x}}_i|\right) \mathbf{j} \equiv f_{1i}\mathbf{i} + f_{2i}\mathbf{j},$$

where

$$|\hat{\vec{x}}_i| = \sqrt{\hat{x}_i^2 + \hat{y}_i^2}.$$

We can now calculate the Jacobian matrix

$$\begin{bmatrix} \frac{\partial f_{1i}}{\partial \hat{x}_i} & \frac{\partial f_{1i}}{\partial \hat{y}_i} \\ \frac{\partial f_{2i}}{\partial \hat{x}_i} & \frac{\partial f_{2i}}{\partial \hat{y}_i} \end{bmatrix},$$

via derivatives:

$$\begin{aligned}
\frac{\partial f_{1i}}{\partial \hat{x}_i} &= \frac{g(|\vec{x}_i|)}{|\vec{x}_i|} + \frac{g'(|\vec{x}_i|)x_i^2}{|\vec{x}_i|^2} - \frac{x_i^2 g(|\vec{x}_i|)}{|\vec{x}_i|^3}, \\
\frac{\partial f_{1i}}{\partial \hat{y}_i} &= \frac{g'(|\vec{x}_i|)x_i y_i}{|\vec{x}_i|^2} - \frac{g(|\vec{x}_i|)x_i y_i}{|\vec{x}_i|^3}, \\
\frac{\partial f_{2i}}{\partial \hat{x}_i} &= \frac{g'(|\vec{x}_i|)x_i y_i}{|\vec{x}_i|^2} - \frac{g(|\vec{x}_i|)x_i y_i}{|\vec{x}_i|^3}, \\
\frac{\partial f_{2i}}{\partial \hat{y}_i} &= \frac{g(|\vec{x}_i|)}{|\vec{x}_i|} + \frac{g'(|\vec{x}_i|)y_i^2}{|\vec{x}_i|^2} - \frac{y_i^2 g(|\vec{x}_i|)}{|\vec{x}_i|^3}.
\end{aligned}$$

Evaluating these matrix entries at the steady state values $(\hat{x}_i,\ \hat{y}_i) = (d, 0)$ gives

$$\begin{aligned}
\frac{\partial f_{1i}}{\partial \hat{x}_i}|_{(d,0)} &= \frac{g(d)}{d} + \frac{g'(d)d^2}{d^2} - \frac{d^2 g(d)}{d^3} = g'(d), \\
\frac{\partial f_{1i}}{\partial \hat{y}_i}|_{(d,0)} &= 0, \\
\frac{\partial f_{2i}}{\partial \hat{x}_i}|_{(d,0)} &= 0, \\
\frac{\partial f_{2i}}{\partial \hat{y}_i}|_{(d,0)} &= \frac{g(d)}{d}.
\end{aligned}$$

Then we can write the Jacobian matrix as

$$\mathbf{D} = \frac{\partial \vec{f}}{\partial \hat{\vec{x}}_i}|_{(d,0)} = \begin{bmatrix} g'(d) & 0 \\ 0 & g(d)/d \end{bmatrix}.$$

With definitions of $\mathbf{\Omega}$ and $\mathbf{RD}$ from (27), we now can write the system in (28).

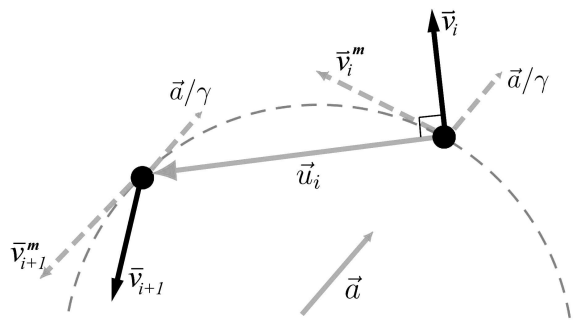

Fig. 15: A schematic diagram of particles at the threshold of mill breaking. The angle between particles is $\pi/2$, beyond which particle i no longer senses particle $i+1$. $\vec{v}_i^{\,m}$ indicates the velocity of particle i in the absence of autonomous self-propulsion.

C Eigenvalue equation

The set of diagonal blocks is given by $D_i = \Lambda + \mathbf{D} + \varpi^{i-1}\mathbf{RD}$, $i = 1, \ldots, n$. We equivalently consider the set D_{i+1}, $i = 0, \ldots, n-1$, for notational ease. Expanding $\det D_{i+1} = 0$ gives

$$
\begin{aligned}
p(\lambda) = &\left(\lambda(\lambda+\gamma) - \omega_0^2 + g'(d) - \exp\left(\frac{2\pi i j}{n}\right)\cos\frac{-2\pi}{n}g'(d)\right)\cdot \\
&\left(\lambda(\lambda+\gamma) - \omega_0^2 + g(d)/d - \exp\left(\frac{2\pi i j}{n}\right)\cos\frac{-2\pi}{n}\frac{g(d)}{d}\right) + \\
&\left(\gamma\omega_0 + 2\lambda\omega_0 + \exp\left(\frac{2\pi i j}{n}\right)\sin\frac{-2\pi}{n}\frac{g(d)}{d}\right)\left(\gamma\omega_0 + 2\lambda\omega_0 + \exp\left(\frac{2\pi i j}{n}\right)\sin\frac{-2\pi}{n}g'(d)\right) = 0.
\end{aligned}
\tag{58}
$$

Using the expression for ω_0 in (16), and for $g(d)/d$ in (29), we reduce the parameters to γ, n, and $g'(d)$, while the index $i = 0, \ldots, n-1$ (corresponding to $D_1, \ldots, D_n$).

D Derivation of Inequality (37)

At the steady state of the moving mill, we have

$$
\vec{v}_i^{\,s} = \omega_0 r_0 \begin{bmatrix} -\sin\left(\hat{\theta}_i(t)\right) \\ \cos\left(\hat{\theta}_i(t)\right) \end{bmatrix} + \frac{\vec{a}}{\gamma}, \qquad \vec{u}_i = \begin{bmatrix} \sin\left(\hat{\theta}_i(t) + \frac{\pi}{n}\right) \\ \cos\left(\hat{\theta}_i(t) + \frac{\pi}{n}\right) \end{bmatrix},
$$

where $\hat{\theta}_i(t) = 2\pi i/n + \omega_0 t$. The threshold of $\vec{a}$ occurs when these two vectors are perpendicular, that is, $\vec{v}_i^s \cdot \vec{u}_i = 0$ (see Figure 15). Expanding this condition gives

$$-\omega_0 r_0 \sin\left(\hat{\theta}_i(t)\right) \sin\left(\hat{\theta}_i(t) + \frac{\pi}{n}\right) - \frac{a_1}{\gamma} \sin\left(\hat{\theta}_i(t) + \frac{\pi}{n}\right) + \tag{59}$$

$$\omega_0 r_0 \cos\left(\hat{\theta}_i(t)\right) \cos\left(\hat{\theta}_i(t) + \frac{\pi}{n}\right) + \frac{a_2}{\gamma} \cos\left(\hat{\theta}_i(t) + \frac{\pi}{n}\right) = 0, \tag{60}$$

where $\vec{a} = [a_1 \;\; a_2]^T$. This equation simplifies using trigonometric identities to

$$\frac{a_1}{\gamma} \sin\left(\hat{\theta}_i(t) + \frac{\pi}{n}\right) - \frac{a_2}{\gamma} \cos\left(\hat{\theta}_i(t) + \frac{\pi}{n}\right) = \omega_0 r_0 \cos\left(\frac{\pi}{n}\right).$$

Using the expressions for ω_0 and r_0 from the existence conditions, we further simplify the threshold condition to

$$a_1 \sin\left(\hat{\theta}_i(t) + \frac{\pi}{n}\right) - a_2 \cos\left(\hat{\theta}_i(t) + \frac{\pi}{n}\right) = \gamma \left(\frac{\gamma \sin(\frac{\pi}{n})}{\cos(\frac{\pi}{n})}\right) \left(\frac{g(d)\cos^2(\frac{\pi}{n})}{\gamma^2 \sin(\frac{\pi}{n})}\right) \cos\left(\frac{\pi}{n}\right), \tag{61}$$

$$= g(d)\cos^2\left(\frac{\pi}{n}\right). \tag{62}$$

Mill breaking actually occurs whenever $\vec{v}_i^s \cdot \vec{u}_i \leq 0$, i.e.,

$$a_1 \sin\left(\hat{\theta}_i(t) + \frac{\pi}{n}\right) - a_2 \cos\left(\hat{\theta}_i(t) + \frac{\pi}{n}\right) \geq g(d)\cos^2\left(\frac{\pi}{n}\right),$$

so we must maximize the left-hand side over all possible angles to find the minimal values of a_1 and a_2 that lead to mill breaking. It can easily be shown using calculus that the left-hand side attains a global maximum value of $|\vec{a}| = \sqrt{a_1^2 + a_2^2}$. This gives our mill breaking condition in (37).

References

[Ben-Jacob *et al.*(1997)] Ben-Jacob, E. *et al.*, 1997. Chemomodulation of cellular movement, collective formation of vortices by swarming bacteria, and colonial development. *Physica A* **238**, 181–197.

[Camazine *et al.*(2001)] Camazine, S. *et al.*, 2001. *Self-organization in biological systems*. Princeton University Press, Princeton.

[Chuang *et al.*(2007)] Chuang, Y. L. *et al.*, 2007. State transitions and the continuum limit for a 2d interacting, self-propelled particle system. *Physica D* **232**, 33–47.

[Couzin *et al.*(2002)] Couzin, I. D. *et al.*, 2002. Collective memory and spatial sorting in animal groups. *J. Theor. Biol.* **218**, 1–11.

[Csahók and Czirók(2008)] Csahók, Z. and A. Czirók, 2008. Hydrodynamics of bacterial motion. *Physica A* **243**, 304–318.

[Czirók *et al.*(1996)] Czirók, A. *et al.*, 1996. Formation of complex bacterial colonies via self-generated vortices. *Phys. Rev. E* **54 2**, 1792–1801.

[Davis(1979)] Davis, P. J., 1979. *Circulant Matrices*. Wiley, New York.

[D'Orsogna *et al.*(2006)] D'Orsogna, M. R. *et al.*, 2006. Self-propelled particles with soft-core interactions: Patterns, stability, and collapse. *Physical Review Letters* **96**, 104302.

[Grossman *et al.*(2008)] Grossman, D., I. S. Aranson and E. Ben-Jacob, 2008. Emergence of agent swarm migration and vortex formation through inelastic collisions. *New Journal of Physics* **023036**.

[Harvey-Clark *et al.*(1999)] Harvey-Clark, C. J. *et al.*, 1999. Putative mating behavior in basking sharks off the Nova Scotia coast. *Copeia* **No. 3**, 780–782.

[Hemmingsson(1995)] Hemmingsson, J., 1995. Modellization of self-propelling particles with a coupled map lattice model. *J. Phys. A* **28**, 4245–4250.

[Huth and Wissel(1992)] Huth, A. and C. Wissel, 1992. The simulation of movement of fish schools. *J theor biol* **156**, 365–385.

[Kulinskii *et al.*(2005)] Kulinskii, V. L. *et al.*, 2005. Hydrodynamic model for a system of self-propelling particles with conservative kinematic constraints. *Europhys. Lett.* **71 (2)**, 207–213.

[Levine *et al.*(2001)] Levine, H., W. Rappel and I. Cohen, 2001. Self-organization in systems of self-propelled particles. *Physical Review E* **63**, 017101.

[Li *et al.*(2007)] Li, Y., R. Lukeman and L. Edelstein-Keshet, 2007. Minimal mechanisms for school formation in self-propelled particles. *Phys. D. (Accepted)* .

[Mach and Schweitzer(2007)] Mach, R. and F. Schweitzer, 2007. Modeling vortex swarming in daphnia. *Bull. Math. Bio.* **69(2)**, 539–562.

[Marshall *et al.*(2004)] Marshall, J. A., M. E. Broucke and B. A. Francis, 2004. Formations of vehicles in cyclic pursuit. *Automatic Control, IEEE Transactions on* **49 (11)**, 1963–1974.

[Mogilner *et al.*(2003)] Mogilner, A. *et al.*, 2003. Mutual interactions, potentials, and individual distance in a social aggregation. *J Math Biol* **47**, 353–389.

[Niwa(1994)] Niwa, H.-S., 1994. Self-organizing dynamic model of fish schooling. *J theor Biol* **171**, 123–136.

[Niwa(1996)] Niwa, H.-S., 1996. Newtonian dynamical approach to fish schooling. *J theor Biol* **181**, 47–63.

[Niwa(1998)] Niwa, H.-S., 1998. Migration of fish schools in heterothermal environments. *J theor Biol* **193**, 215–231.

[Okubo(1980)] Okubo, A., 1980. *Diffusion and Ecological Problems: Mathematical Models.* Springer Verlag, New York.

[Okubo *et al.*(2001)] Okubo, A., D. Grunbaum and L. Edelstein-Keshet, 2001. The dynamics of animal grouping. In A. Okubo and S. Levin (eds.), *Diffusion and Ecological Problems: Modern Perspectives*, chapter 7. Springer, N.Y.

[Parr(1927)] Parr, A. E., 1927. A contribution to the theoretical analysis of the schooling behaviour of fishes. *Occasional Papers of the Bingham Oceanographic Collection* **1**, 1–32.

[Parrish and Edelstein-Keshet(1999)] Parrish, J. and L. Edelstein-Keshet, 1999. Complexity, pattern, and evolutionary trade-offs in animal aggregation. *Science* **284**, 99–101.

[Parrish *et al.*(2002)] Parrish, J., S. Viscido and D. Grunbaum, 2002. Self-organized fish schools: an examination of emergent properties. *Biol. Bull.* **202**, 296–305.

[Ratushnaya *et al.*(2007)] Ratushnaya, V. I. *et al.*, 2007. Stability properties of the collective stationary motion of self-propelling particles with conservative kinematic constraints. *J. Phys. A* **40**, 2573–2581.

[Sakai(1973)] Sakai, S., 1973. A model for group structure and its behavior. *Biophysics Japan* **13**, 82–90.

[Schneirla(1944)] Schneirla, T. C., 1944. A unique case of circular milling in ants, considered in relation to trail following and the general problem of orientation. *American Museum Novitates* **1253**, 1–25.

[Silvester(2000)] Silvester, J. R., 2000. Determinants of block matrices. *Maths Gazette* **84**, 460–467.

[Suzuki and Sakai(1973)] Suzuki, R. and S. Sakai, 1973. Movement of a group of animals. *Biophysics Japan* **13**, 281–282.

[Topaz and Bertozzi(2004)] Topaz, C. and A. Bertozzi, 2004. Swarming patterns in a two-dimensional kinematic model for biological groups. *SIAM J. Appl. Math.* **65 (1)**, 152–174.

[Vicsek *et al.*(1995)] Vicsek, T. *et al.*, 1995. Novel type of phase transition in a system of self-driven particles. *Phys. Rev. Lett.* **75(6)**, 1226–1229.

[Weihs(1974)] Weihs, D., 1974. Energetic advantages of burst swimming of fish. *J. theor. Biol.* **48**, 215–229.

[Wilson(2004)] Wilson, S. G., 2004. Basking sharks schooling in the southern Gulf of Maine. *Fish. Oceanogr.* **13**.